



저작자표시-비영리-변경금지 2.0 대한민국

이용자는 아래의 조건을 따르는 경우에 한하여 자유롭게

- 이 저작물을 복제, 배포, 전송, 전시, 공연 및 방송할 수 있습니다.

다음과 같은 조건을 따라야 합니다:



저작자표시. 귀하는 원저작자를 표시하여야 합니다.



비영리. 귀하는 이 저작물을 영리 목적으로 이용할 수 없습니다.



변경금지. 귀하는 이 저작물을 개작, 변형 또는 가공할 수 없습니다.

- 귀하는, 이 저작물의 재이용이나 배포의 경우, 이 저작물에 적용된 이용허락조건을 명확하게 나타내어야 합니다.
- 저작권자로부터 별도의 허가를 받으면 이러한 조건들은 적용되지 않습니다.

저작권법에 따른 이용자의 권리는 위의 내용에 의하여 영향을 받지 않습니다.

이것은 [이용허락규약\(Legal Code\)](#)을 이해하기 쉽게 요약한 것입니다.

[Disclaimer](#)

이학박사학위논문

포도당 결핍에 의한 오토파지 유도
상황에서 PHF20의 전사 조절 기작에
대한 연구

Studies on the Transcriptional Regulation of Glucose
Starvation Induced Autophagy by PHF20

2022년 8월

서울대학교 대학원

생명과학부

박 세 원

Studies on the Transcriptional Regulation of Glucose Starvation Induced Autophagy by PHF20

by

Se Won Park

Advisor

Professor Sung Hee Baek, Ph.D.

A Thesis for the Degree of Doctor of Philosophy

August, 2022

School of Biological Sciences

Seoul National University

포도당 결핍에 의한 오토파지 유도 상황에서 PHF20의 전사 조절 기작에 대한 연구

Studies on the Transcriptional Regulation
of Glucose Starvation Induced autophagy by PHF20

지도교수 백 성 희

이 논문을 이학 박사 학위논문으로 제출함
2022년 7월

서울대학교 대학원
생명과학부
박 세 원

박세원의 박사학위 논문을 인준함
2022년 7월

위 원 장	_____ (인)
부 위 원 장	_____ (인)
위 원	_____ (인)
위 원	_____ (인)
위 원	_____ (인)

**Studies on the Transcriptional Regulation
of Glucose Starvation Induced autophagy
by PHF20**

*A dissertation submitted in partial fulfillment of
the requirement for the degree of*

DOCTOR OF PHILOSOPHY

TO THE FACULTY of
THE SCHOOL of BIOLOGICAL SCIENCES
at
SEOUL NATIONAL UNIVERSITY
by

Se Won Park

Date approved

ABSTRACT

Se Won Park
School of Biological Sciences
The Graduate School
Seoul National University

Autophagy is a catabolic pathway that maintains cellular homeostasis under various stress conditions, including conditions of nutrient deprivation. To elevate autophagic flux to a sufficient level under stress conditions, transcriptional activation of autophagy genes occurs to replenish autophagy components. Thus, the transcriptional and epigenetic control of the genes regulating autophagy is essential for cellular homeostasis. Here, I applied integrated transcriptomic and epigenomic profiling to reveal the roles of plant homeodomain finger protein 20 (PHF20), which is an epigenetic reader possessing methyl binding activity, in controlling the expression of autophagy genes. Phf20 deficiency led to impaired autophagic flux and autophagy gene expression under glucose starvation. Interestingly, the genome-wide characterization of chromatin states by Assay for Transposase-Accessible Chromatin (ATAC)-sequencing revealed that the PHF20-dependent chromatin remodelling occurs in enhancers that are co-occupied by dimethylated lysine 36 on

histone H3 (H3K36me2). Importantly, the recognition of H3K36me2 by PHF20 was found to be highly correlated with increased levels of H3K4me1/2 at the enhancer regions. Collectively, these results indicate that PHF20 regulates autophagy genes through enhancer activation via H3K36me2 recognition as an epigenetic reader. Our findings emphasize the importance of nuclear events in the regulation of autophagy.

This work was published in Se Won Park, Jaehoon Kim, Sungryong Oh, Jeongyoon Lee, Joowon Cha, Hyun Sik Lee, Keun Il Kim, Daechan Park, Sung Hee Baek, PHF20 is crucial for epigenetic control of starvation-induced autophagy through enhancer activation, *Nucleic Acids Research*, 2022;, gkac584. Permission to adapt the contents of the publication was acquired from the co-authors.

Key words

Epigenetics, Autophagy, Glucose starvation, Plant Homeodomain Finger 20 (PHF20), Enhancer, Histone methylation, mixed-lineage leukemia protein (MLL) complex

Student Number: 2015-20429

CONTENTS

	Page
ABSTRACT	i
CONTENTS	iii
LIST OF FIGURES AND TABLES	vi
CHAPTER I. Introduction	1
I-1. Autophagy	2
1.1. Autophagy in cellular homeostasis	2
1.2. Transcriptional regulation of autophagy	4
I-2. Plant Homeodomain Finger 20 (PHF20)	6
2.1. Epigenetic reader molecule and PHD finger protein family	6
2.2. Structure and function of PHF20	8
I-3. Enhancer	10
3.1. Enhancers in gene regulation	10
3.2. Histone markers of enhancers	13

I-4. MLL complex	13
4.1. MLL complex and histone methylation	13
4.2. Subtypes of MLL complexes	14

CHAPTER II. PHF20 is crucial for starvation induced autophagy related gene activation

II-1. Summary	17
II-2. Introduction	18
II-3. Results	21
II-4. Discussion	45
II-5. Materials and Methods	46

CHAPTER III. PHF20 activates autophagy enhancers via the recognition of H3K36me2 and the recruitment of mixed lineage leukemia 3/4 (MLL3/4) complex	54
III-1. Summary	55
III-2. Introduction	56
III-3. Results	58
III-4. Discussion	76
III-5. Materials and Methods	79
 CHAPTER IV. Conclusion	 86
REFERENCES	89
국문초록 / ABSTRACT IN KOREAN	101

LIST OF FIGURES AND TABLES

Figure I-1. Illustration of autophagy process and autophagy inducing stresses	3
Figure I-2. Epigenetic regulation of autophagy process	5
Figure I-3. Illustration of epigenetic regulation and structure of PHF20	9
Figure I-4. Process of enhancer activation	11
Figure I-5. Subtypes of MLL complexes	15
Figure II-1. Biochemical assays for autophagy	20
Figure II-2. LC3 conversion is decreased in <i>Phf20</i> ^{-/-} MEFs under various autophagy inducing signals	22
Figure II-3. GFP-LC3 puncta formation is decreased in <i>Phf20</i> ^{-/-} MEFs under glucose starvation	23
Figure II-4. Autophagy flux is decreased in <i>Phf20</i> ^{-/-} under glucose starvation	25
Figure II-5. RNA-seq reveals effects of PHF20 in transcription regulation	28

Figure II-6 Expression pattern of each k -means cluster	29
Figure II-7. PHF20 induces autophagy genes under glucose starvation	31
Figure II-8. PHF20 functions as a transcriptional coactivator of autophagy genes	33
Figure II-9. PHF20 affects to exchange of chromatin structure under glucose starvation	35
Figure II-10. PHF20 affects to chromatin opening of autophagy related genes	36
Figure II-11. ChromHMM classifies genome into 16 different states	38
Table II-1. The distribution of genome within the chromHMM states	39
Figure II-12. Average profiles of DOPs per state in chromHMM	41
Figure II-13. State 6, 7 and 8 in chromHMM show PHF20 dependent opening pattern	42
Figure II-14. PHF20 activates autophagy genes through chromatin opening	44

Figure III-1. PHF20 dependent chromHMM states correlate with H3K36 methylation	58
Figure III-2. PHF20 Tudor domain binds H3K36me2	60
Figure III-3. PHF20 is recruited to target region by Tudor domain	61
Figure III-4. PHF20 is recruited to target region via recognition of H3K36me2 by Tudor domain	62
Figure III-5. <i>Phf20</i> deletion reduces active enhancer markers on its target DOPs	64
Figure III-6. <i>Phf20</i> deletion reduces active enhancer markers on its target DOPs closely located to autophagy related genes	65
Figure III-7. PHF20 binds MLL3/4 complex	67
Figure III-8. PHF20 recruits MLL3/4 complex to the target enhancers	69
Figure III-9. Expression of eRNA on target enhancer is induced by PHF20	70
Figure III-10. Activity of PHF20 dependent DOP affects to expression of autophagy related genes	72

Figure III-11. Enhancer-promoter looping occurs between PHF20 dependent DOPs and promoters of autophagy related genes	74
Figure III-12. PHF20 is crucial for epigenetic regulation of autophagy via H3K36me2-dependent enhancer activation.	75

CHAPTER I

Introduction

I-1. Autophagy

1.1 Autophagy in cellular homeostasis

Autophagy is a catabolic pathway that maintains cellular homeostasis under various stress conditions, including conditions of nutrient deprivation. Autophagy is a highly conserved process that maintains cellular homeostasis by eliminating unnecessary proteins and damaged organelles (Klionsky and Emr, 2000; Mizushima et al., 2008). Under stress conditions such as nutrient starvation, autophagy is highly induced to perform a cytoprotective function (Lum et al., 2005; Yang and Klionsky, 2010). Since autophagy is essential for both cell survival and protection against various types of environmental damage, dysregulated autophagy can cause serious human diseases, including diabetes, neurodegenerative diseases, and cancer (Choi et al., 2013; Levine and Kroemer, 2008).

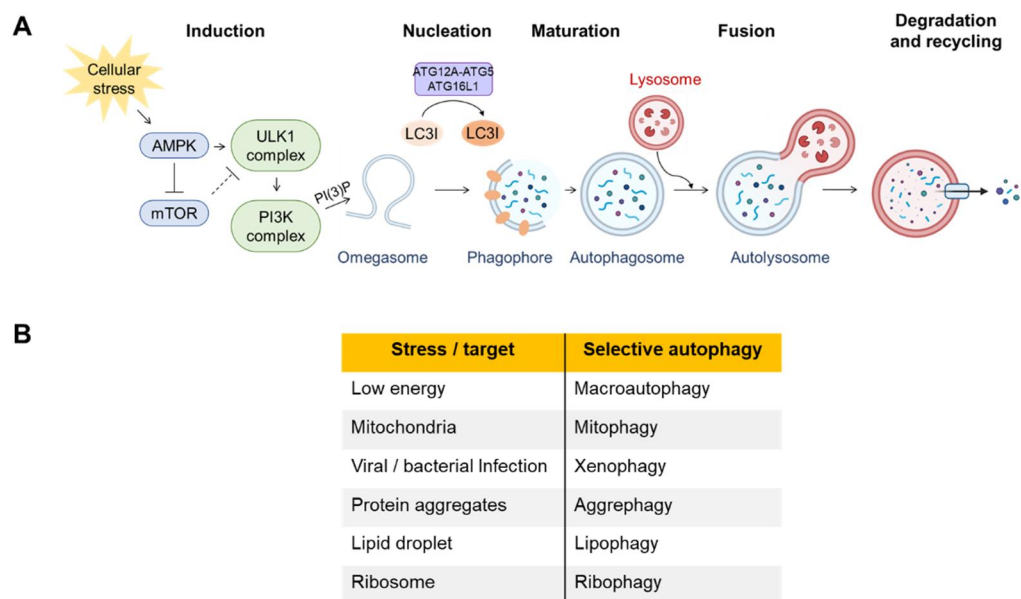


Figure I-1. Illustration of Autophagy process and Autophagy inducing stress

(A) Illustration of Autophagy process. Omegasome induced by various cellular stress undergoes nucleation, maturation, lysosome fusion to create autolysosome. (B) Autophagy inducing cellular stresses and according selective autophagy

1.2 Transcriptional regulation of autophagy

As autophagy proceeds, the protein components of autophagosomes, along with their autophagy cargoes, are rapidly degraded by lysosomes (Glick et al., 2010; Mizushima, 2007). Thus, the transcription of autophagy components should be increased to avoid the depletion of the autophagosome and to maintain an optimal autophagic flux under cellular stress conditions (Baek and Kim, 2017; Fullgrabe et al., 2014). Previous studies have mainly reported the functions of transcription factors, including transcription factor EB (TFEB) and the forkhead box O (FOXO) protein family, to be involved in the regulation of autophagy (Mammucari et al., 2007; Settembre et al., 2011; Zhou et al., 2012). TFEB recognizes the CACGTG sequence in DNA (the “CLEAR” motif), and activates the transcription of its specific target genes, including autophagy and lysosomal genes. Moreover, alterations of histone modification on promoters of autophagy target genes also play important role for transcriptional regulation of autophagy. For example, H3R17me2 levels are increased by coactivator-associated arginine methyltransferase 1 (CARM1) under glucose starvation conditions, thereby leading to the activation of TFEB target genes (Shin et al., 2016). In contrast, H4K16ac levels are reduced by decreased Males absent on the first (MOF) histone acetyltransferase activity and sirtuin 1 activation upon autophagic stimulation.

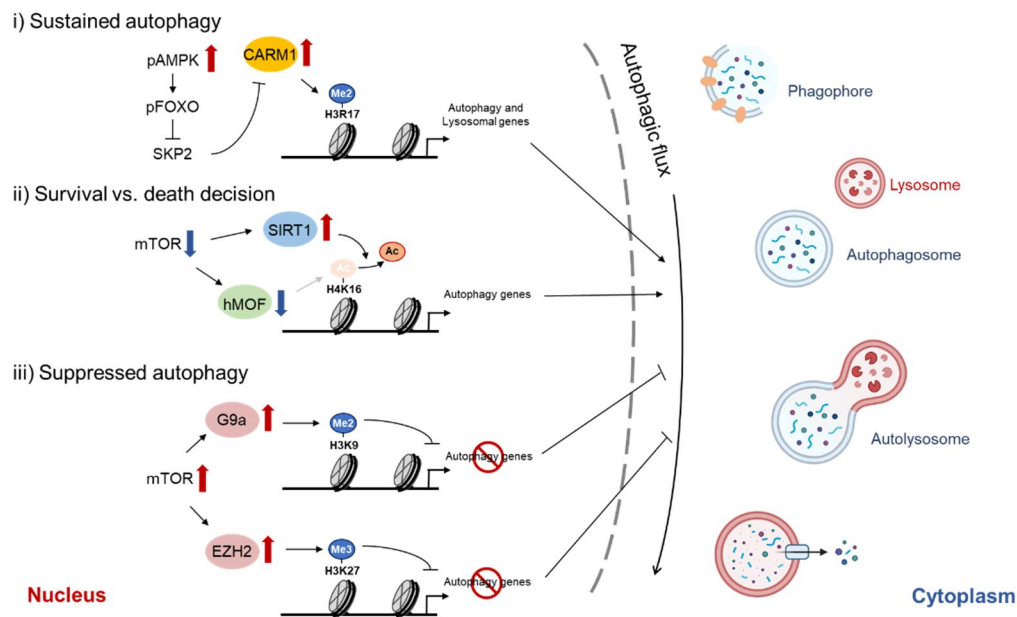


Figure I-2. Epigenetic regulation of autophagy process

i) In sustained autophagy, E3 ligase SKP2 is decreased by activated AMPK pathway. In turn, the arginine methyltransferase CARM1, which is substrate of SKP2, is increased and induces H3R17me2 on promoters of Autophagy and Lysosomal genes. ii) To decide survival or death faith of cells, downregulated mTOR pathway decreases H4K16 acetyltransferase hMOF and increases H4K16 deacetylase SIRT1. iii) To suppress autophagy process, activated mTOR increase expression of methyltransferases G9a and EZH2. G9a induces H3K9 methylation and EZH2 increases H3K27 trimethylation on autophagy genes. All of these epigenetic regulations orchestrate to control cytoplasmic autophagy events.

I-2. Plant Homeodomain Finger 20 (PHF20)

2.1. Epigenetic reader molecule and PHD finger protein family

The epigenetic regulation of gene expression is controlled by three class of regulators: writer, eraser and reader. First, epigenetic writers establish specific histone modifications on target sites with enzymatic activity (Biswas and Rao, 2018). In contrast, epigenetic erasers delete existing histone modifications from target sites. For example, histone methyltransferases induce methylation on target sites, while histone demethylases erase methylations (Alam et al., 2015; Greer and Shi, 2012). Since the balance between writer and eraser is crucial to establish appropriate histone modification at correct situation, their expression or activity have to be tightly regulated by signaling cascade. On the other hands, epigenetic reader molecules directly interacts with confined histone repertoire (Yun et al., 2011). They have specific domain that can recognizes certain types of histone modification. Some of reader molecules have intrinsic enzymatic activity that can exchange epigenetic status on target sites, and other reader molecules just function as scaffold protein which brings another effector complexes to target sites (Hyun et al., 2017).

As an epigenetic reader molecule, PHD finger protein family members recognize various histone modifications including methylation and acetylation. PHF1 recognizes symmetrically di-methylated H4R3 (H4R3me₂s) and interacts with CUL4B-Ring E3 ligase complex (Liu et al., 2018). PHF19 directly recognizes H3K27me₃ and recruits PRC2 complex to target sites. PHF19 is also required for the full enzymatic activity of PRC2

complex (Ballare et al., 2012).

Moreover, some PHFs reported to have intrinsic E3 ligase activity and directly induces histone ubiquitination. In post-meiotic spermatid, PHF7 function as an E3 ubiquitin ligase for histone H3K14 (Kim et al., 2020). Another PHD finger protein family PHF6 is an E3 ubiquitin ligase for H2BK120 and plays important role in trophectodermal gene expression (Oh et al., 2020). PHF15, as known as JADE-2, induces degradation of LSD1 via its E3 ubiquitin ligase activity during neurogenesis (Han et al., 2014).

2.2. Structure and function of PHF20

PHF20, a member of the PHF family, contains two conserved Tudor domains and one plant homeodomain (PHD) (Cui et al., 2012). As a core component of MOF-nonspecific lethal (NSL) protein complex, PHF20 recognizes methylation of histone or non-histone targets and recruits NSL complex to target promoters, thereby enhancing histone H4 acetylation (Cai et al., 2010; Li et al., 2009; Shia et al., 2006; Taipale et al., 2005). PHF20 recognizes H3K4me2 through PHD and recruits NSL complex to H3K4me2 enriched active promoters (Klein et al., 2016). Moreover, PHF20 interacts with methyl residues on non-histone proteins, including estrogen receptor α , p53, and p65 through Tudor domains (Zhang et al., 2013; Zhang et al., 2016), and also recruits NSL complex to target genes occupied by methylated ER α , p53 or p65.

In one study, *Phf20*-deficient (*Phf20*^{-/-}) mice reported to show a high rate of perinatal lethality, with the surviving adults having a smaller body size than the wild-type (WT) mice, which is a well-known characteristic of autophagy-defective mice (Badeaux et al., 2012).

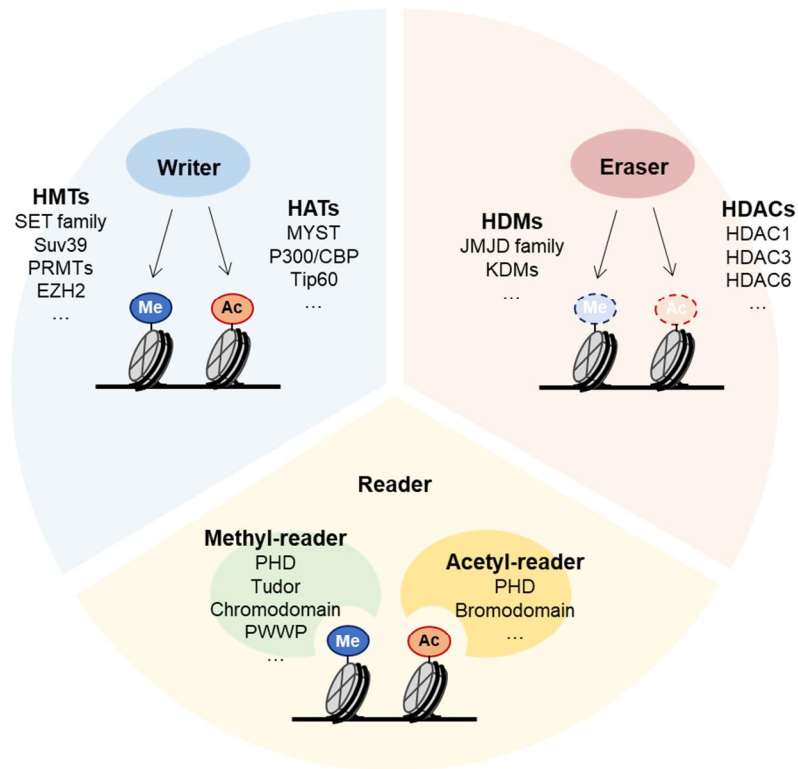
A**B**

Figure I-3. Illustration of epigenetic regulation and structure of PHF20

(A) Epigenetic writer, eraser and reader proteins regulates gene expression through alteration of histone modification. (B) The domain structures of PHF20

I-3. Enhancer

3.1. Enhancers in gene regulation

An enhancer is a cis-acting regulatory DNA region which can be located up to 1 Mbp away from its target promoter. Active enhancer is usually bound by transcription factors and plays functions for inducing target gene expression in various situations. Generally, core promoters alone have low basal activity and need assist from other cis-regulatory elements for sufficient gene expression. As major cis-regulatory elements, enhancers control cell-type or signal-specific gene regulation and can increase target gene expressions up to 100-fold. In many cases, activated enhancers are physically contacted with their target promoters. Between active enhancer and its target promoter, chromatin looping is driven by the cohesin complex and leads long-range interaction. Once contact is made, looping is stabilized by other connector proteins including CTCF or YY1. additional binding of cell-type or signal-specific transcription factors is also occurred to fully achieve enhancer-promoter interaction. Especially, enhancer is controlled by the specific combination of DNA-binding proteins including transcription factors to precisely regulate gene expression patterns. For example, expression of HOX family proteins controls which enhancers will be activated at specific spatial and temporal developmental stage.

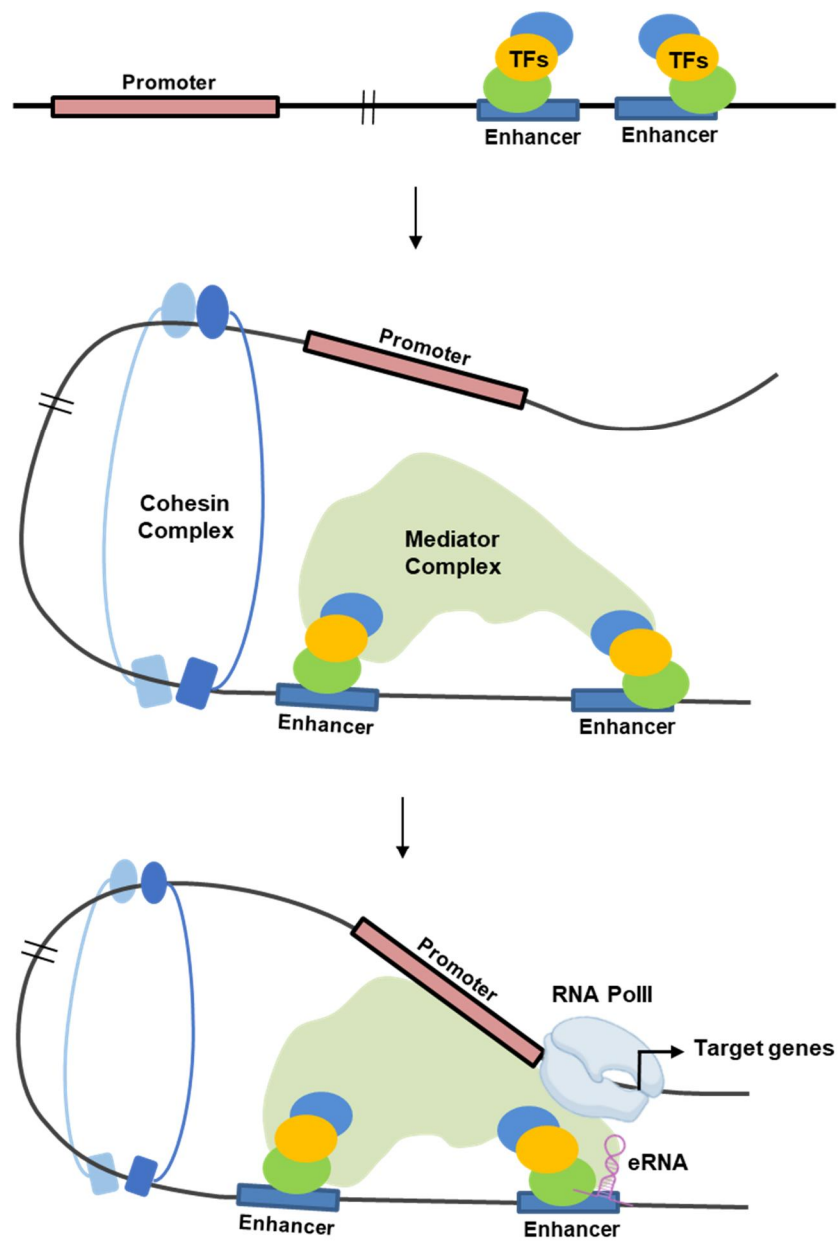


Figure I-4. Process of enhancer activation

3.2. Histone markers of enhancers

Like other genome regions, enhancers exhibit characteristic histone modifications. At the initial stage of enhancer activation, MLL3 and MLL4 are recruited to the enhancer by transcription factors and establish H3K4 monomethylation. Acetylation on Histone H3K27 is another well-known hallmark of active enhancers. This modification might reflect the presence of histone acetyl-transferase (HAT) complex at active enhancer regions. Intriguingly, highly activated enhancers are enriched both H3K4me1 and H3K27ac while enhancers with H3K4me1 only are classified as 'poised' enhancers. Such poised enhancers are involved in early stage of enhancer activation and undergoes further activation by environmental signals like developmental cues.

I-4. MLL complex

4.1. MLL complex and histone methylation

Among the various histone methylations, H3K4 methylation is known to be closely related to active transcription, and highly enriched at the promoters, transcription start sites and active enhancers (Miller et al., 2001; Shilatifard, 2012). The function of H3K4 methylation and the enzymes which regulate H3K4 methylation are highly evolutionarily conserved. From yeast to mammalian, SET1 family methyltransferases have an important role for H3K4 methylation.

SET1 family methyltransferases including the MLL family proteins should be associated with WRAD components—which comprise WDR5, RbBP5, Ash2L and DPY-30—for their complete activation (Ernst and Vakoc, 2012; Miller *et al.*, 2001). WRAD induces the allosteric activation of methyltransferases or recruits methyltransferases to the appropriate target sites (Bryk et al., 2010; Patel et al., 2009; Patel et al., 2011; Steward et al., 2006). For example, the SET domain of MLL1 alone only shows weak activity for H3K4 monomethylation, but interaction with WRAD complex allows MLL1 to induce H3K4 dimethylation with more

4.2. Subtypes of MLL complexes

Although all MLL complexes are responsible for H3K4 methylation, their detailed regulatory mechanism differs between each subtype. MLL complexes share WRAD complex as common components which make methyltransferase fully activated, while each complex has unique additional subunits depends on subtype of methyltransferase. For MLL1/2 (also known as KMT2A/B), additional subunit Menin plays regulatory roles. Otherwise, MLL3/4 (also known as KMT2C/D) complex has four additional subunits; UTX, PTIP, NCOA6 and PA1.

Since the MLL complex is responsible for all three types of H3K4 methylations, each subtype of MLL complex possesses distinct enzymatic activity toward its substrate; MLL1/2 is a major methyltransferase for H3K4me3 on promoters (Hu et al., 2013; Wang et al., 2009), while MLL3/4 is responsible for the accumulation of H3K4me1 on active enhancers (Herz et al., 2012; Lee et al., 2013; Liu et al., 2019). Therefore, the genomic site where each subtype of the MLL complex is recruited under specific conditions should be tightly regulated.

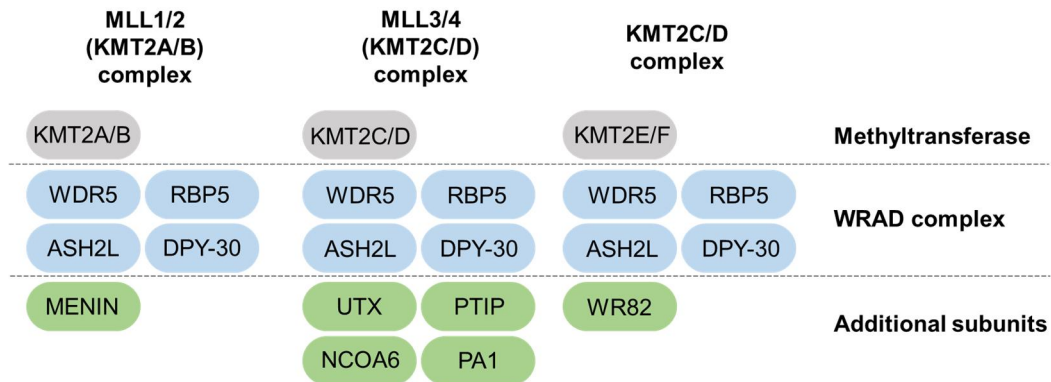


Figure I-5. Subtypes of MLL complexes

Hippo pathway is highly conserved kinase cascade which is composed of MST1/2, LATS1/2 kinase and YAP/TAZ transcriptional co-activator. When MST1/2 is inactivated, the YAP/TAZ co-activators translocate into the nucleus to activate TEAD transcription factor. When MST1/2 is activated and activates its downstream LATS1/2, the YAP/TAZ co-activators is phosphorylated and they are sequestered in cytoplasm or degraded.

CHAPTER II

PHF20 is crucial for starvation induced autophagy related gene activation

II-1. Summary

As an epigenetic reader protein, PHF20 is known to be involved in various transcription regulatory processes through its methylation-binding affinity. Because *Phf20*^{-/-} mice show similar phenotypes with autophagy deficient mice including perinatal lethality and developmental disorders, I hypothesized that PHF20 is crucial for autophagy induction via its transcription activating function.

Here, I found that PHF20 deficiency causes decreased autophagy flux under glucose starvation. mRNA expression of autophagy related genes should be increased under glucose starvation to compensate continuous degradation of autophagosome organizing proteins. RNA-sequencing data showed that autophagy related genes were not induced in *Phf20*^{-/-} Mouse Embryonic Fibroblasts (MEFs). Also, ATAC-sequencing revealed that chromatin structure undergoes global alteration by PHF20 depletion. Especially, I classified total genome regions into 16 states using chromHMM, and found PHF20 dependent chromatin regions were concentrated specific genome state. At last, by integrating analysis of RNA-seq and ATAC-seq, I identified that PHF20 dependent chromatin structure exchange is directly correlated with PHF20 dependent gene expression pattern.

I investigated autophagy related genes as novel target of PHF20 under glucose starvation from these data. Moreover, effect of PHF20 on genome-wide chromatin structure in ATAC-seq gave an important insight for gene regulatory mechanism of PHF20.

II-2. Introduction

Biochemical assays for autophagy

As autophagy occurs, microtubule-associated protein 1A/1B-light chain 3 (LC3-I) is transformed to LC3-II which is phosphatidylethanolamine conjugated form of LC3-I. LC3-II then is incorporated to autophagosome membrane and functions as a binding platform for other autophagosomal proteins including autophagy cargo receptors. Autophagy can be detected biochemically using those characteristics of LC3. First, the relative amount of LC3-II can be detected by western-blotting. Cytosolic form of LC3-I is at size of 17kDa with western blot assay. However, as lipid phosphatidylethanolamine is conjugated to LC3-I to form LC3-II, size of LC3 is shifted to about 12kDa. By comparing intensities of those two bands on western blot, the cellular amount of autophagosome can be predicted. Moreover, autophagosome incorporated LC3 also can be detected by immunocytochemistry. As cells are stained with endogenous LC3 antibody or overexpressed with GFP tagged LC3, cellular LC3 can be detected with a fluorescence microscopy. If cells undergo autophagy process, the autophagosome incorporated LC3-II is detected as puncta under microscopy and those puncta can be counted to compare intensity of autophagy. Furthermore, mCherry-GFP-LC3 construct can be used to detect autophagosome/autolysosome with fluorescence microscopy. During the formation of an autophagosome, mCherry-GFP-LC3 conjugates with the autophagosome membrane and

stains the vesicle yellow, which results from the fluorescence of both mCherry and GFP. After a lysosome fuses with an autophagosome to form an autolysosome, only red fluorescence is observed, because the fluorescent activity of GFP is vulnerable to the acidic environment.

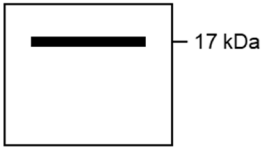
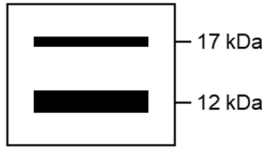

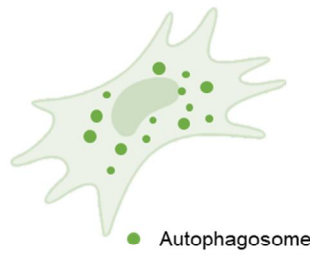

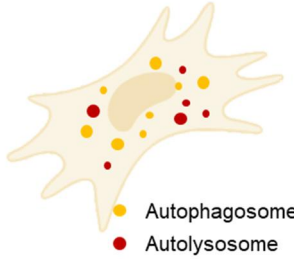
	Basal Autophagy	Induced Autophagy
LC3 conversion		
GFP-LC3 Puncta formation		
mCherry-GFP-LC3 Puncta formation		

Figure II-1 Biochemical assays for autophagy

II-3. Results

***Phf20* deletion reduces LC3 conversion by autophagy inducing signals**

As the phenotypes of *Phf20*^{-/-} mice showing perinatal lethality are often observed for autophagy-defective mice, I tested the possibility that PHF20 is involved in autophagy. To detect autophagic activity, I analyzed the conversion of non-lipidated light chain 3 (LC3)-I form to lipidated LC3-II form, which is a common marker of autophagic occurrence. I induced autophagy in WT and *Phf20*^{-/-} mouse embryonic fibroblasts (MEFs) by glucose and amino acid starvation, and found that LC3-II conversion in *Phf20*^{-/-} MEFs was attenuated as compared to that in WT MEFs under both glucose and amino acid starvation conditions (Figure II-2A and 2B). The same results were observed upon rapamycin treatment, which induces autophagy by inhibiting mammalian target of rapamycin (mTOR) (Figure II-2C).

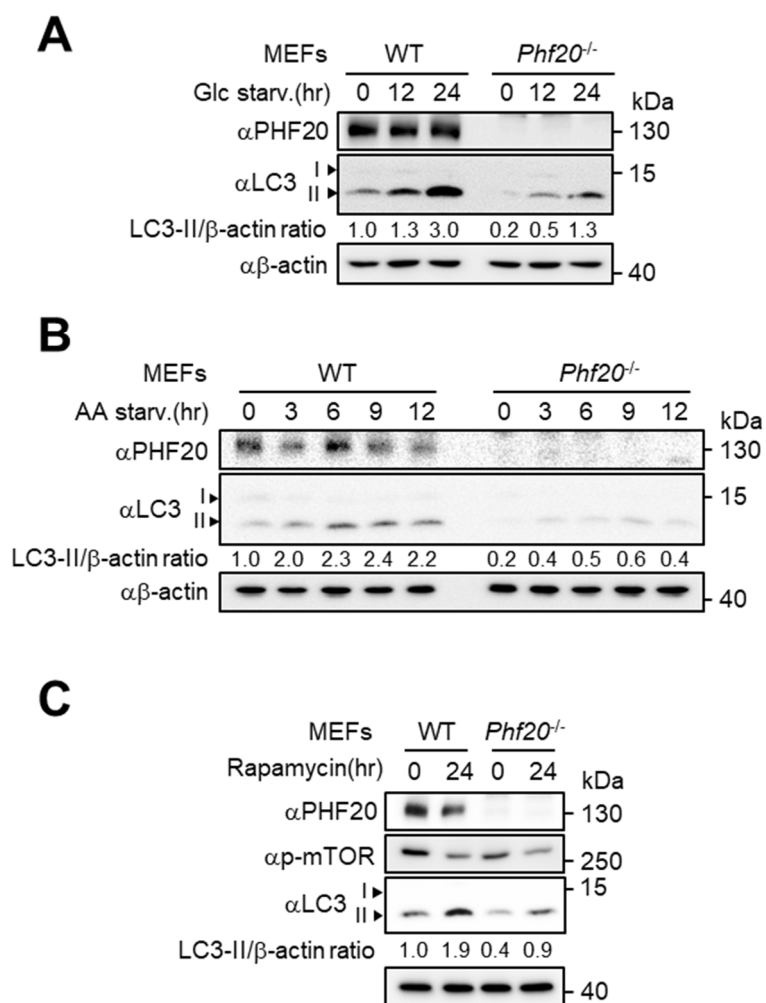


Figure II-2. LC3 conversion is decreased in *Phf20*^{-/-} MEFs under various autophagy inducing signals

Immunoblot analysis of light chain 3 (LC3) levels in cell lysates of WT or *Phf20*^{-/-} MEFs after glucose starvation (**A**), amino acid starvation (**B**), and rapamycin (150 nM) treatment (**C**). The number below indicates LC3-II/ β -actin ratio.

***Phf20* deletion reduces GFP-LC3 puncta formation under glucose starvation**

The formation of green fluorescent protein (GFP)-tagged LC3-positive autophagosomes was examined to evaluate the role of PHF20 in autophagy. Upon glucose starvation, the number of GFP-LC3 punctate cells increased in WT MEFs, however, this increase in number of puncta was attenuated in *Phf20*^{-/-} MEFs (Figure II-3).

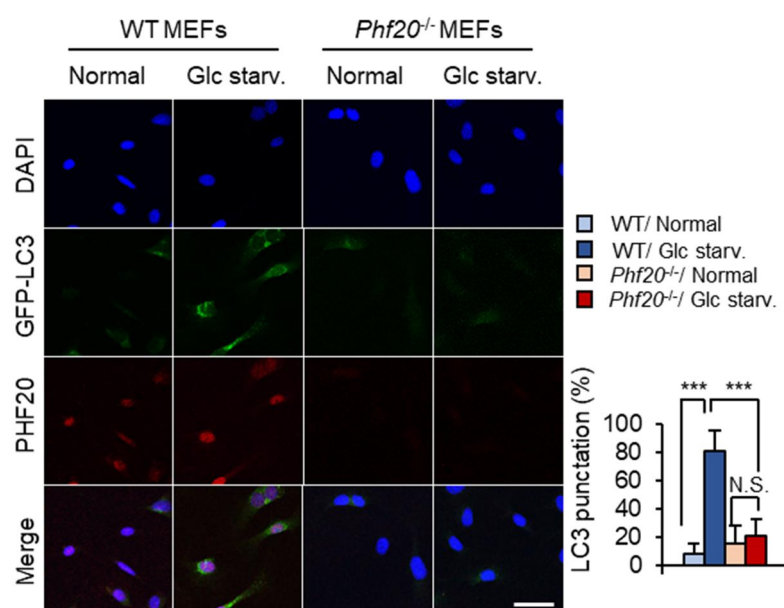


Figure II-3. GFP-LC3 puncta formation is decreased in *Phf20*^{-/-} MEFs under glucose starvation.

Representative confocal images of GFP-LC3 puncta formed under control or glucose starvation conditions. Scale bar, 50 μ m. The graph indicates the number of LC3-positive cells. Bars, mean \pm standard error of the mean (SEM); *** p < 0.001. Statistical analysis using two-tailed t-test.

***Phf20* deletion reduces autophagy flux under glucose starvation**

Next, I compared the autophagic flux between WT and *Phf20*^{-/-} MEFs by treating the cells with lysosomal inhibitors that prevent the degradation of the mature autophagosome. I treated WT and *Phf20*^{-/-} MEFs with chloroquine (CQ) and compared the induction of autophagic flux in the cells under glucose starvation (Figure II-4A). While the autophagic flux in WT MEFs was greatly increased by glucose starvation, *Phf20*^{-/-} MEFs failed to show significant increase in autophagic flux (Figure II-4A). Similar results were observed in the absence or presence of Bafilomycin A treatment with Cyto-ID staining, which is an autophagosome-specific fluorescent reporter (Figure II-4B). The number of autophagosomes was increased to a much higher extent by glucose starvation in WT MEFs than in *Phf20*^{-/-} MEFs. Thereafter, I used the mCherry-GFP-LC3 reporter to examine the total number of autophagosomes induced and the extent of autophagic flux at the same time. Consecutively, WT MEFs showed increased number of both yellow and red puncta under glucose starvation, whereas *Phf20*^{-/-} MEFs had significantly attenuated number of both puncta (Figure II-4C). Therefore, these results indicate that *Phf20* deficiency impairs the induction of autophagic flux under glucose starvation.

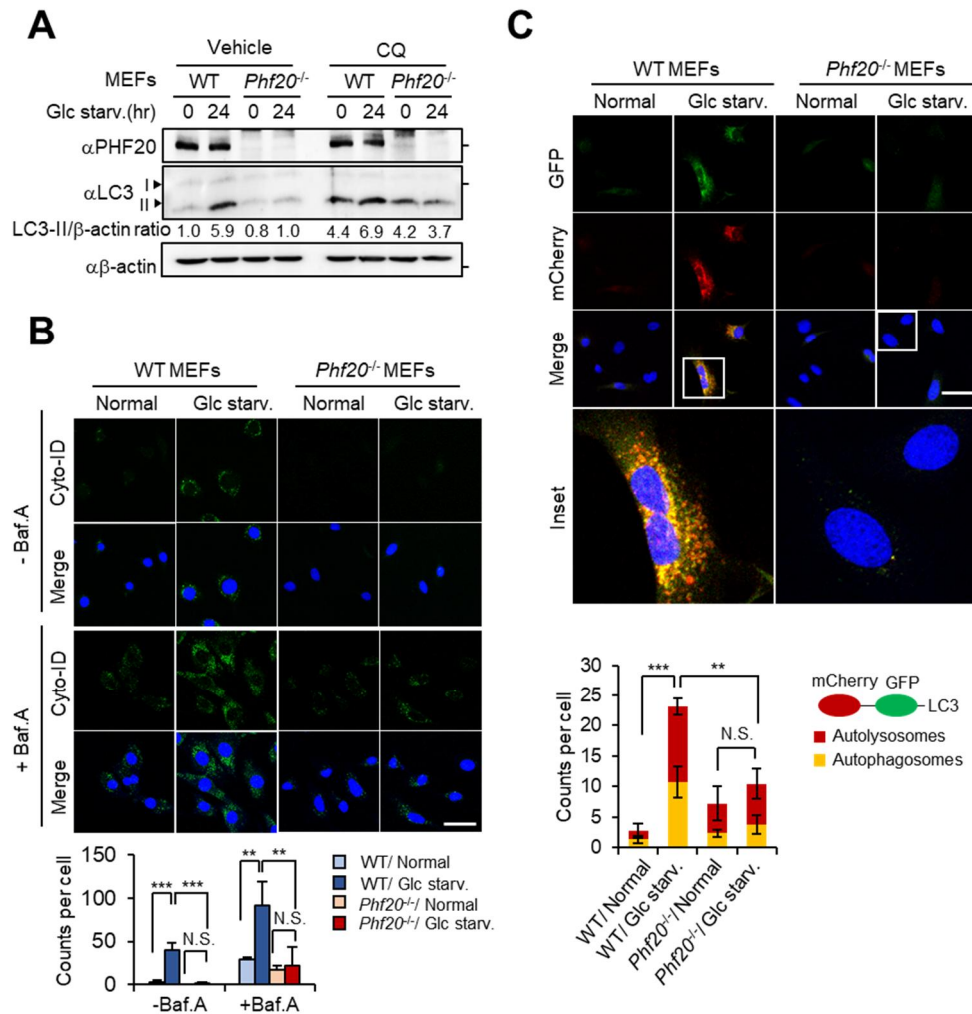


Figure II-4. Autophagy flux is decreased in *Phf20*^{-/-} under glucose starvation

(A) Autophagic flux was analyzed in WT or *Phf20*^{-/-} MEFs in the presence or absence chloroquine (10 μM; 4 h) under glucose starvation conditions. The LC3-II/β-actin ratio is indicated. (B) Representative confocal images of autophagic vacuoles in WT or *Phf20*^{-/-} MEFs in the presence or absence of bafilomycin A1 (200 nM; 2 h). Autophagic vacuoles were detected using the CYTO-ID staining. Nucleus are stained with Hoechst (Blue). Scale bar, 50 μm. The graph indicates the number of autophagic vacuoles per cells. Bars, mean ± SEM; ** p < 0.01, *** p < 0.001. Statistical analysis using two-tailed t-test. (C)

Representative confocal images of mCherry-GFP-LC3 assays in WT or *Phf20*^{-/-} MEFs. Colocalization of mCherry and GFP signal (yellow puncta) represents autophagosomal vesicles that have not fused with a lysosomal compartment (phagophores or autophagosomes). mCherry signal without GFP signal (red puncta) represents acidic autophagosomal vesicles (acidic amphisomes or autolysosomes). Nucleus are stained with DAPI (Blue). Scale bar, 50 μ m. The graph indicates the number of puncta per cell. Bars, mean \pm SEM; ** $p < 0.01$, *** $p < 0.001$. Statistical analysis using two-tailed t-test.

PHF20 functions as a transcriptional regulator under glucose starvation

To examine the role of PHF20 in autophagy at the transcriptional level, I carried out RNA-sequencing (RNA-seq) of WT and *Phf20*^{-/-} MEFs with or without glucose starvation (Figure II-5A). In unsupervised hierarchical clustering, the *Phf20*^{-/-} MEFs were closely clustered independent of the starvation conditions, thereby suggesting that Phf20 deletion eliminates the transcriptional responses to glucose starvation (Figure II-5B). I then performed *k*-means clustering (*k* = 8) to figure out the functional role of PHF20 in regulating gene expression (Figure II-5C). The genes in cluster 1 were expressed in a PHF20-dependent manner, as the deletion of Phf20 led to the failure of activation of the genes in WT MEFs upon glucose starvation (Figure II-6).

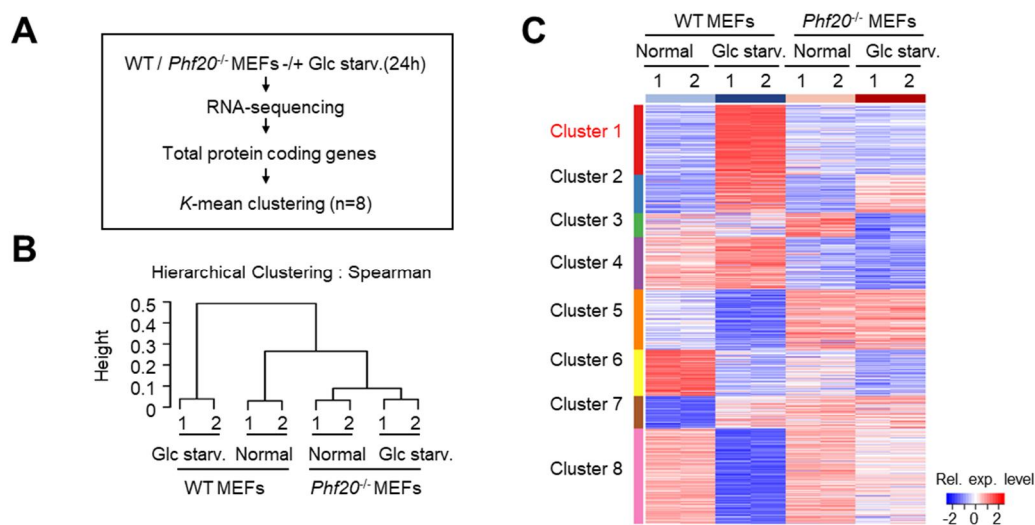


Figure II-5. RNA-seq reveals effects of PHF20 in transcription regulation

(A) Workflow of RNA-sequencing and downstream analysis. (B) Unsupervised hierarchical clustering using top 10 % variably expressed genes. The y-axis shows distance in Spearman correlation coefficient. (C) Heat map of *k*-means clustering of total protein coding genes in WT and *Phf20*^{-/-} with or without glucose starvation (n = 12208, k = 8). The genes are clustered in 8 different groups based on relative gene expression across the samples. Cluster 1 which shows PHF20 dependent gene activation pattern is highlighted in red.

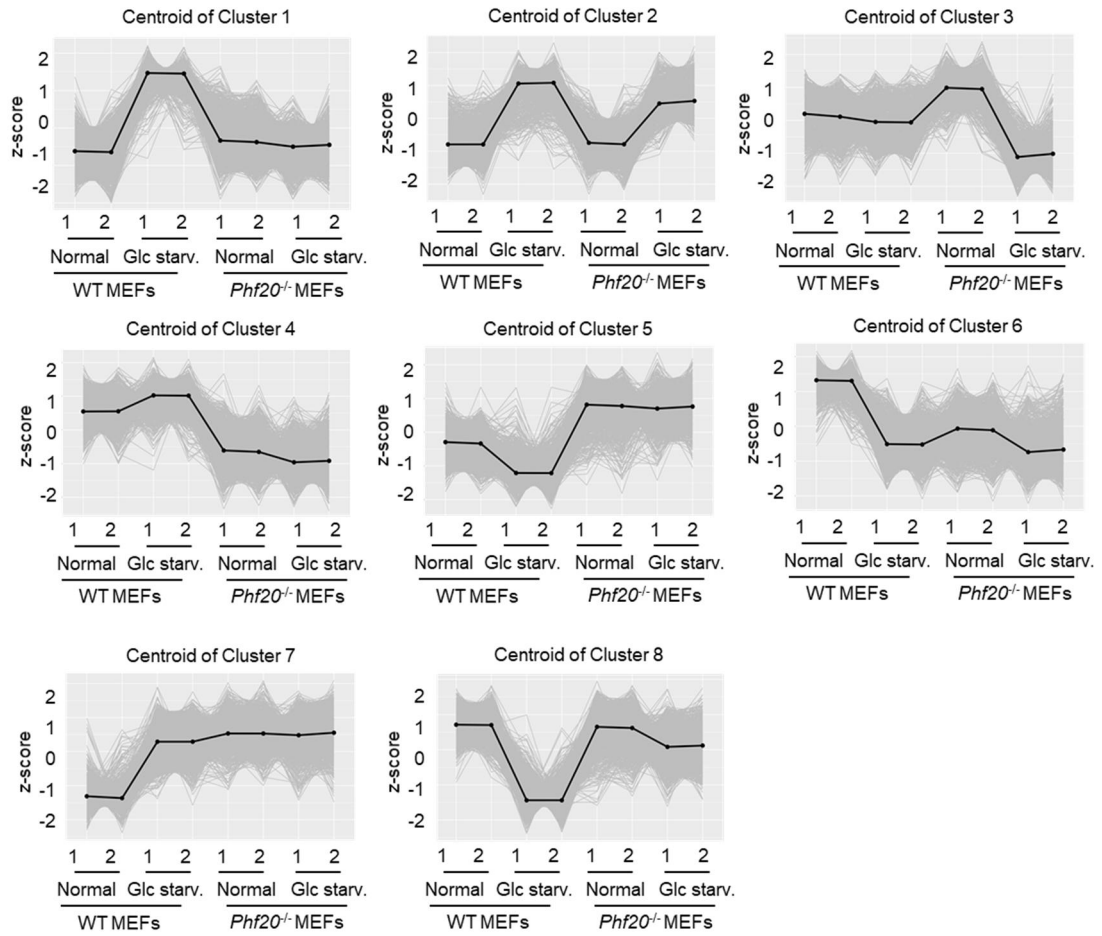


Figure II-6. Expression pattern of each k -means cluster

z-score centroids of each k -means Cluster. The black line and grey lines indicate the centroid and genes, respectively.

PHF20 is required for the induction of autophagy related genes under glucose starvation

Interestingly, gene ontology (GO) analysis revealed that autophagy genes were significantly represented in cluster 1, indicating that PHF20 is involved in transcriptional activation of autophagy genes (Figure 2E). Next, I conducted gene set enrichment analysis (GSEA) by ranking the genes based on Pearson correlation coefficient in a PHF20-dependent manner. The results confirmed that the gene sets of the autophagic process were significantly enriched in the PHF20-dependent cluster (Figure 2F).

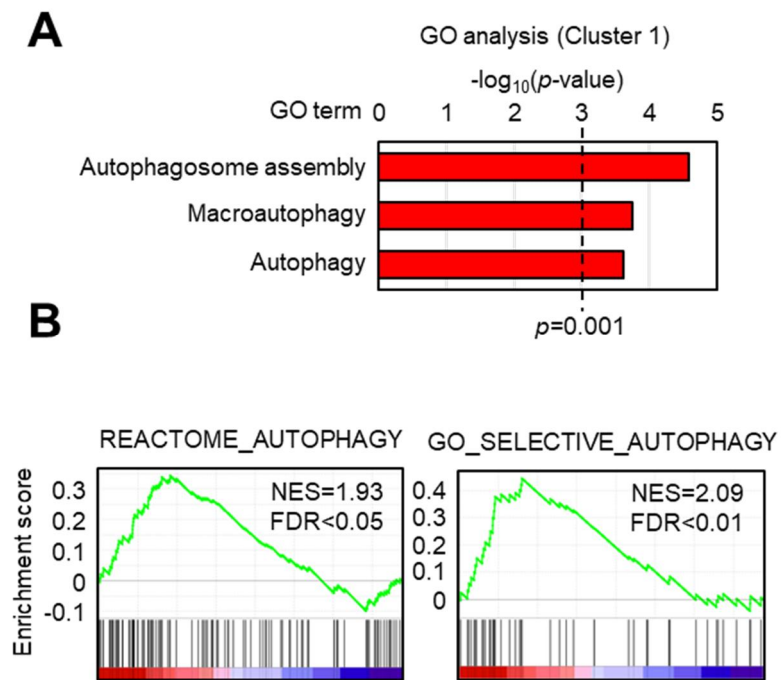


Figure II-7. PHF20 induces autophagy genes under glucose starvation

(A) Functional Gene Ontology (GO) analysis on the genes in Cluster 1. Autophagy related terms are shown significantly in Cluster 1 but not in other clusters. (B) Gene Set Enrichment Analysis (GSEA) for the genes correlated with the gene expression in Cluster 1. FDR, false discovery rate; NES, normalized enrichment score.

Furthermore, I observed that the activation of genes related to autophagy initiation, phagophore expansion, and cargo recruitment and trafficking (85) in WT MEFs upon glucose starvation was repressed by Phf20 deletion, thereby showing the transcriptional dependency of autophagy on PHF20 (Figure 2G). I further validated the function of PHF20 in transcriptional regulation using quantitative real-time polymerase chain reaction (qRT-PCR) for the genes associated with autophagy such as those encoding the autophagy (Atg) family proteins and the autophagy receptor sequestosome 1 (Sqstm1), also known as p62 (Figure 2H). Taken together, the results of gene expression profiling revealed that PHF20 acts as a transcriptional coactivator during autophagy on a transcriptome-wide scale.

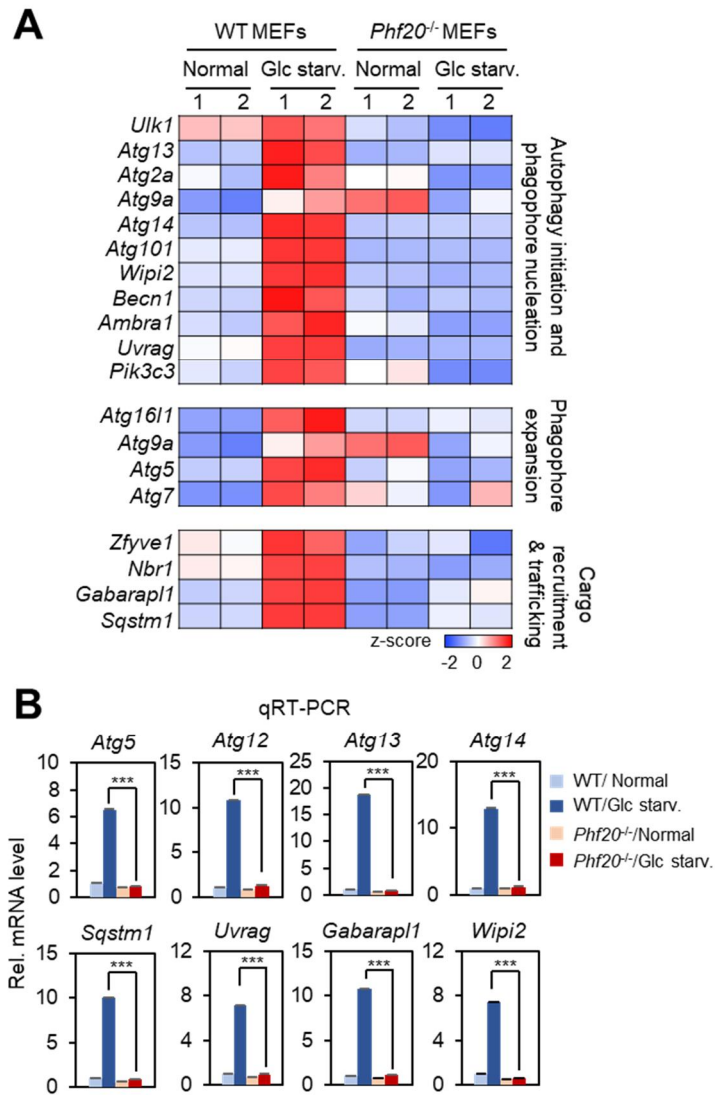


Figure II-8. PHF20 functions as a transcriptional coactivator of autophagy genes

(A) Expression levels of genes involved in autophagy initiation, phagophore expansion, and cargo recruitment and trafficking. (B) mRNA expression of autophagy-related genes with quantitative real time-PCR (qRT-PCR). Bars, mean \pm SEM; *** $p < 0.001$. Statistical analysis using two-tailed t-test.

PHF20 modulates chromatin structure under glucose starvation

As PHF20 is a chromatin-binding protein, I carried out ATAC-seq to elucidate the role of PHF20 in the alteration of chromatin structures during autophagy (Figure II-9A). After peak calling for open chromatin regions in ATAC-seq, hierarchical clustering using the peak intensities showed that clusters were segregated between WT and *Phf20*^{-/-} (Figure II-9B). The dendrogram in Figure 3B indicates that open chromatin structures were globally altered by *Phf20* deletion, whereas the effect of glucose starvation on chromatin structures was relatively minimal. I then identified differentially opening peaks (DOPs) between WT and *Phf20*^{-/-} under each condition. I observed that 16,976 and 20,906 peaks were significantly changed by *Phf20* deletion under normal and glucose starvation condition, respectively (Figure II-9C).

Next, I conducted GO term analysis on the genes which show starvation-induced chromatin opening peaks (Figure II-10). The results showed that autophagy-related GO terms were significantly represented in WT MEFs, indicating a PHF20-dependent chromatin opening of autophagy-related genes under glucose starvation.

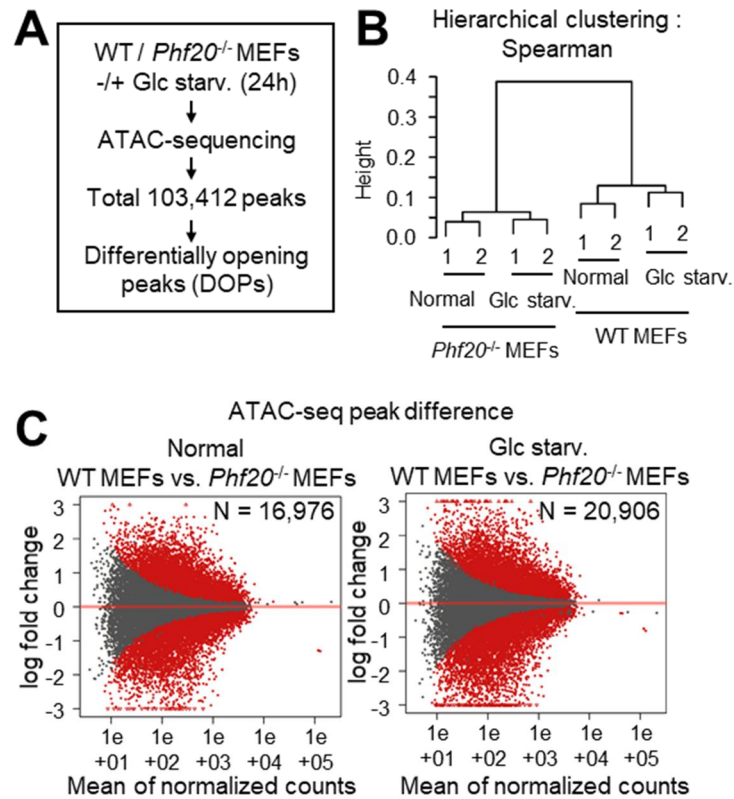


Figure II-9. PHF20 affects to exchange of chromatin structure under glucose starvation

(A) Workflow of ATAC-sequencing analysis. (B) Unsupervised hierarchical clustering using top 10 % variably opened peaks (Spearman distance). The height implies similarity of opening peaks by each sample. (C) Differentially opening peaks (DOPs) between WT and *Phf20*^{-/-} under each condition. Red dots represent statistically significant DOPs that are less than adjusted *p*-value 0.05. N, the number of DOPs that are greater than fold change 2 and less than adjusted *p*-value 0.05.

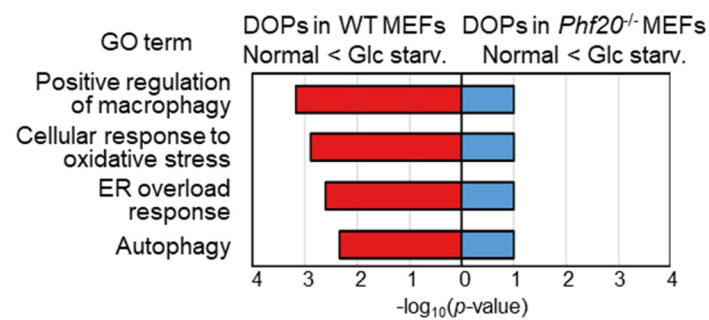


Figure II-10. PHF20 affects to chromatin opening of autophagy related genes

Functional analysis for the DOPs between conditions. GO results are shown for the genes whose TSS are within 10 kb from the DOPs. Autophagy-related terms are significantly found in WT but not *Phf20*^{-/-}.

ChromHMM reveals characteristics of PHF20 dependent chromatin regions

To investigate precisely which chromatin states were regulated by PHF20 on a genome-wide scale, I utilized chromHMM, which is a software for discovering chromatin states by learning chromatin signatures based on the multivariate Hidden Markov Model (Ernst and Kellis, 2012; 2017). I collected 12 different publicly available ChIP-seq datasets, such as RNA polymerase II and CTCF ChIP-seq datasets, and various histone ChIP-seq datasets derived from studies using MEFs (Figure II-11). After learning the diverse chromatin signatures, I were able to generate genome-wide chromatin annotations consisting of 16 states (Table II-1).

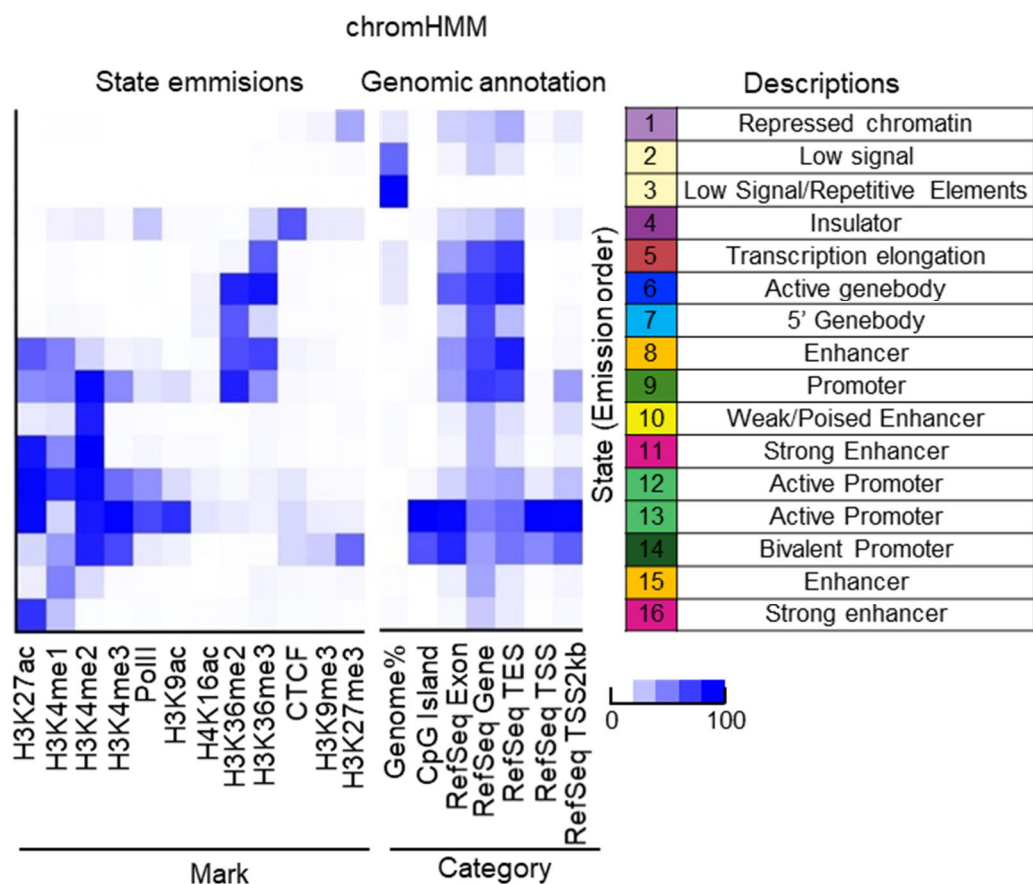


Figure II-11. ChromHMM classifies genome into 16 different states

Chromatin state using chromHMM software. Each row represents one chromatin state. From left to right: Histone mark and probability used to define the states (State emission). Chromatin state enrichment in genomic features (Genomic annotation). Description of 16 states (Descriptions). (F) Average plots of DOPs in state 6, 7 and 8 by each sample.

State	Description	Whole region (Mbp)	DOPs
1	Repressed chromatin	131	1,287
2	Low signal	775	8,933
3	Low Signal/Repetitive Elements	1,286	2,523
4	Insulator	11	633
5	Transcription elongation	143	1,255
6	Active genebody	137	950
7	5' Genebody	37	456
8	Enhancer	23	2,082
9	Promoter	14	626
10	Weak/Poised Enhancer	35	4,358
11	Strong Enhancer	32	8,802
12	Active Promoter	14	3,264
13	Active Promoter	22	1,081
14	Bivalent Promoter	11	1,702
15	Enhancer	22	3,016
16	Strong enhancer	40	7,579

Table II-1. The distribution of genome within the chromHMM states

Total length and the number of DOPs for each chromHMM states are indicated.

To specify the chromatin states regulated by PHF20, I calculated the average profile of the DOPs for each state (Figure III-12). I found that states 6, 7 and 8 show relatively strong dependency on PHF20 for starvation-induced chromatin opening, defining PHF20 dependency as states where chromatin became less accessible by *Phf20* depletion under glucose starvation. The state 3 was excluded because it was a repetitive region and had no significant signal of all histone marks. Regarding the states 4, 5, and 9, they exhibited relatively weak PHF20 dependency, meaning that the chromatin accessibility difference (WT Glc starv - KO Glc starv) was smaller. As a result, I finally defined the states 6, 7 and 8 as PHF20-dependent states (Figure III-13).

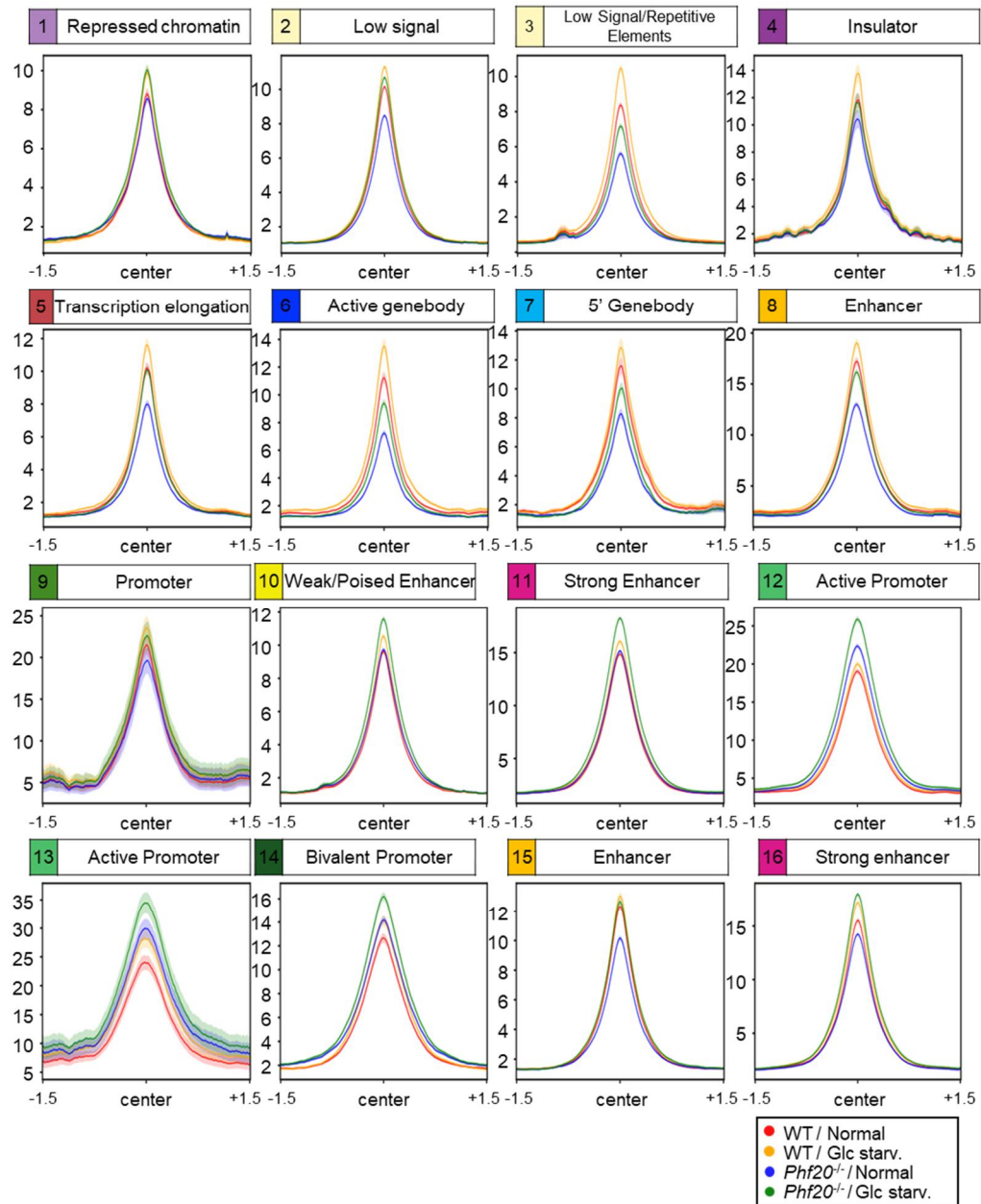
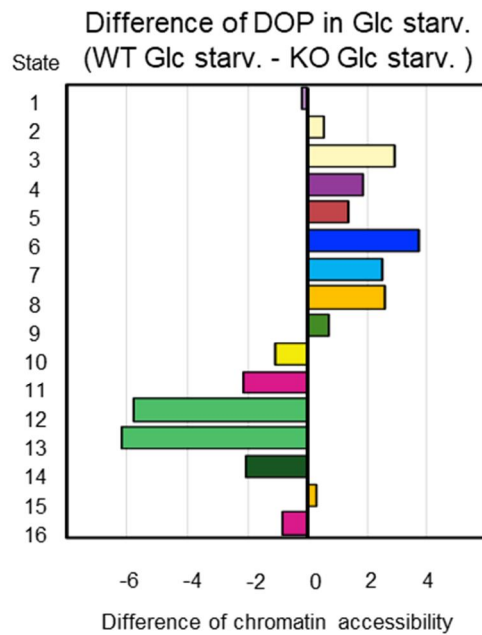


Figure II-12. Average profiles of DOPs per state in chromHMM

Average plots of DOPs in each chromHMM state

A



B

State	Description	Repeat region (%)
1	Repressed chromatin	31.3
2	Low signal	43.0
3	Low signal / Repetitive Elements	51.0
4	Insulator	44.5
5	Transcription elongation	35.0
6	Active genebody	29.5
7	5' Genebody	34.5
8	Enhancer	24.1
9	Promoter	20.7
10	Weak/Poised Enhancer	21.1
11	Strong Enhancer	20.2
12	Active Promoter	16.0
13	Active Promoter	10.7
14	Bivalent Promoter	10.2
15	Enhancer	24.5
16	Strong enhancer	32.9

Figure II-13. State 6, 7 and 8 in chromHMM show PHF20 dependent opening pattern

(A) Difference on Differentially opening peaks (DOPs) between WT and *Phf20*^{-/-} under Glc starv. condition. (B) Repeat region of chromHMM states

PHF20 activates autophagy genes via opening chromatin structure of target regions

Based on the opened patterns of the DOPs along with the chromHMM states, I hypothesized that DOPs in states 6, 7 and 8 lead to the PHF20-dependent gene expression under glucose starvation. To confirm this, I performed an integrative analysis of ATAC-seq with the gene clusters from RNA-seq, which were distinguished by PHF20-dependent gene expression patterns. First, I counted the number of DOPs within 50 kb from the transcriptional start site (TSS) of each gene. Next, I compared the proportions of DOPs between RNA-seq clusters. Interestingly, states 6 and 8 had greater proportion of DOPs in the RNA-seq cluster with PHF20-dependent expression (cluster 1) (Figure II-14), indicating that PHF20-dependent expression is regulated by DOPs in states 6 and 8 near their TSSs (< 50 kb). Collectively, these results indicate that PHF20 activates its target DOPs under glucose starvation, and activation of these DOPs is closely related to the PHF20-dependent expression of autophagy genes.

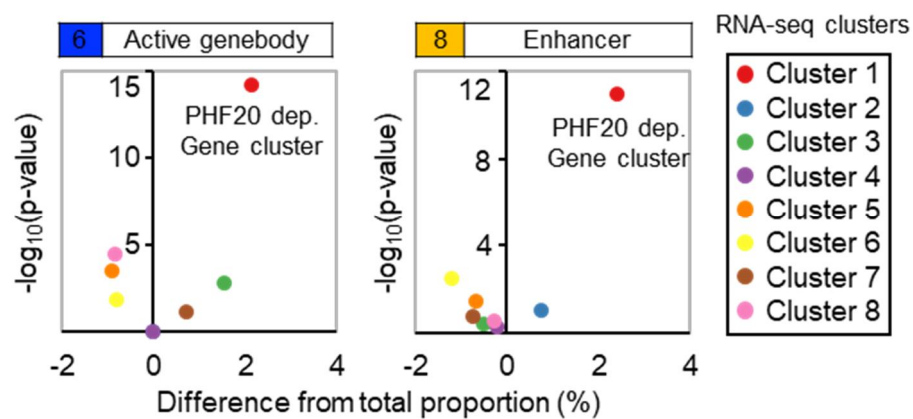


Figure II-14. PHF20 activates autophagy genes through chromatin opening

Comparing the chromHMM state ratio of DOPs in each RNA-sequencing cluster to the ratio of DOPs ($n=33,443$) in total protein-coding genes. DOPs distributed under 50kb from TSS are counted. Statistical analysis using chi-square test. Total protein-coding genes have 4.43 % ($n=1481$ from 33,443 total DOPs, < 50 kb) of state 6 DOPs, and 7.54 % ($n=2521$ from 33,443 total DOPs, < 50 kb) of state 8 DOPs.

II-4. Discussion

Replenishment of autophagy proteins by transcriptional activation is an essential process for prolonged autophagy. This process is achieved by maintaining adequate levels of autophagic flux. To precisely control the expression of specific target genes, epigenetic regulation is crucial. Here, I defined the integrated signaling pathway that connects the upstream inducing signal of autophagy to the downstream target gene expression through epigenetic regulation. Integrative analysis of RNA-seq and ATAC-seq results showed that PHF20 altered the chromatin structure to activate the transcription of autophagy-related genes on a genome-wide scale and the global chromatin opening by PHF20 was more prominent under glucose starvation. With respect to its region of activity on the genome, enhancers and gene bodies were the chromatin states where PHF20 evidently worked, suggesting that PHF20 is likely associated with long range interactions in the 3D genome structure. These specificities of PHF20 for chromatin states were expected to be achieved by interaction with the modified histone marks because each chromHMM state has unique pattern of histone modifications.

I found that there are huge differences in chromatin opening and gene expression between wild type and *Phf20*^{-/-} MEFs through genome-wide sequencing data. This result reflects the importance of PHF20 in global gene expression pattern. Moreover, I achieved unbiased, in-depth analysis genome-wide data with chromHMM, which is computational learning method for chromatin states. With a number of public ChIP-seq data, chromHMM analysis in this study provide detailed information for chromatin states.

II-5. Materials and Methods

Reagents

The following antibodies were used in this study: anti-Flag (F3165) and anti- α -actin (A1978) (Sigma-Aldrich, St. Louis, MO, USA); anti-GFP (sc-9996) and anti-Lamin A/C (sc-6215) (Santa Cruz biotechnology, Dallas, TX, USA); anti-Tubulin (LF-PA0146A) (AbFrontier, Seoul, Korea); anti-PHF20 (#3934), anti-WDR5 (#13105), and anti-LC3 (#2775) (Cell Signaling Technology, Danvers, MA, USA); anti-HA (#MMS-101R) (Covance, Princeton, NJ, USA); Alexa Fluor 488 donkey anti-rabbit IgG (A21206) and Alexa Fluor 594 donkey anti-mouse IgG (A21203) (Invitrogen, Waltham, MA, USA). The following chemicals were used: hygromycin (H3274), puromycin (P8833), and CQ (C6628) (Sigma-Aldrich, St. Louis, MO, USA); Bafilomycin A1 (#11038) (Cayman, Ann Arbor, MI, USA); and rapamycin (R-5000) (LC laboratories, Woburn, MA, USA).

Cell culture and transfection

I generated *Phf20*^{-/-} immortalized mouse embryonic fibroblasts (MEFs) by using 3T3 protocol. WT and *Phf20*^{-/-} MEFs were cultured at 37 °C in Dulbecco's modified Eagle

medium (DMEM) (SH30243.01, HyClone, Marlborough, MA, USA) supplemented with 10 % fetal bovine serum (FBS) (SH30084.03, HyClone) and ZellShield® (13-0050, Minerva biolabs, Hillsborough, NJ, USA) in a humidified incubator with 5 % CO₂. For glucose or amino acid starvation, cells were washed with pre-warmed Dulbecco's phosphate-buffered saline (DPBS) (SH30028.02, HyClone) and then exchanged media with glucose-free DMEM (LM001-56, Welgene, Gyeongsan-si, Korea) or amino acid-free DMEM (LM001-90, Welgene) supplemented with 10 % dialyzed FBS (26400044, Gibco, Amarillo, TX, USA) and ZellShield®. Following reagents were used for cellular transfection: TurboFect (#R0531, ThermoFisher, Waltham, MA, USA) and Lipofectamine 3000 (L3000-001, Invitrogen). All cell lines were maintained without mycoplasma contamination.

Preparation for obtaining whole-cell lysates

To harvest cells, cells were briefly rinsed with cold PBS and collected from the plate with scraper. Then, cells were resuspended in EBC200 buffer (150 mM NaCl, 1 % Triton X-100, 1 % sodium deoxycholate, 0.1 % sodium dodecyl sulfate (SDS), 50 mM Tris-HCl [pH 7.5], and 2 mM ethylenediaminetetraacetic acid (EDTA)) supplemented with protease inhibitors and sonicated using a Branson Sonifier 450 (Branson, Brookfield, CT, USA) at

output 3 and a duty cycle of 30 for 10 pulses. Protein concentration in each lysate was quantified with the Bradford method and normalized with same concentration.

Autophagic vacuole staining

Autophagic vacuoles were stained using the CYTO-ID® autophagy detection kit (ENZ-51031, Enzo Life Sciences, Farmingdale, NY, USA) and observed through fluorescence microscopy. Cells grown on coverslips at a density of 2×10^4 cells were incubated with DMEM containing CYTO-ID® green detection reagent (1:500) and Hoechst 33342 (1:1000) at 37 °C for 30 min. After staining, the cells were washed with PBS and then fixed with 2 % paraformaldehyde in PBS at 20-22 °C for 10 min. Cells were then mounted and visualized under a confocal microscope (LSM700, Zeiss, Oberkochen, Germany).

Immunofluorescence

Cells grown on coverslips at a density of 5×10^4 cells were washed with PBS and then fixed with 2 % paraformaldehyde in PBS at 20-22 °C for 10 min. Fixed cells were permeabilized with 0.5 % Triton X-100 in PBS (PBS-T) and incubated at 20-22 °C for 10 min. Blocking was performed with 3 % bovine serum in PBS-T for 1 h. For staining, the cells were

incubated with antibodies at 20-22 °C for 2 h, followed by incubation with fluorescent-labeled secondary antibodies for 1 h. Cells were then mounted and visualized under a confocal microscope (LSM700, Zeiss). For autophagy studies, MEFs were transfected with GFP-LC3 or mCherry-GFP-LC3 and sub-cultured onto coverslips. The following day, cells were incubated with complete media or glucose-starved media for 18 h.

RNA purification and quantitative real-time PCR (qRT-PCR)

Total RNAs were purified with Trizol (15596026, Invitrogen). Purified RNAs were reverse-transcribed using SuPrimeScript cDNA Synthesis Kit (SRK-1000, GeNetBio, Daejeon, Korea). The reaction was performed with 2.5 µg of purified RNAs as template, Oligo dT and random hexamer for primer. Quantitative RT-PCR was reacted with SYBR TOPreal qPCR 2X PreMix (RT501, Enzynomics, Daejeon, Korea) following manufacturer's protocol. SYBR green signal was detected by an ABI prism 7500 system (Applied Biosystems, Waltham, MA, USA). Abundance of mRNA was quantified by the ddCt method using expression of HPRT, β -actin as control. All reactions were performed as triplicates. The following primers were used for qRT-PCR.

β -actin forward (fwd) 5' -TAGCCATCCAGGCTGTGCTG-3'

Reverse (rev) 5' -CAGGATCTTCATGAGGTAGTC-3'

Hprt	fwd	5' -GCTGGTGAAAAGGACCTCTCG-3'
	rev	5' -CCACAGGACTAGAACACCTGC-3'
Phf20	fwd	5' -GGCTTACTGGAAGAAAACGTGCC-3'
	rev	5' -GCTCAGCCACTCCTTGTCATAC-3'
Map1lc3b	fwd	5' -CACTGCTCTGTCTTGTGTAGGTTG-3'
	rev	5' -TCGTTGTGCCTTTATTAGTGCATC-3'
Atg5	fwd	5' -ATATCAGACCACGACGGAGC-3'
	rev	5' -TTGGCTCTATCCCGTGAATC-3'
Atg12	fwd	5' -TCCGTGCCATCACATACACA -3'
	rev	5' -AGGGCCTTCTTTGCTTCATG-3'
Atg13	fwd	5' -ATTTGCACCCGCTCATCATC-3'
	rev	5' -AGGGCCTTCTTTGCTTCATG-3'
Atg14	fwd	5' -AAGCATGGTGAGCAAGCTTG-3'
	rev	5' -ATGCTAATGCTGGTGTCACC-3'
Sqstm1	fwd	5' -ATGTGGAACATGGAGGGAAGA-3'
	rev	5' -GGAGTTCACCTGTAGATGGGT-3'

Uvrag fwd 5' -ACATCGCTGCTCGGAACATT -3'
rev 5' -CTCCACGTCGGATTCAAGGAA-3'

Gabarapl1 fwd 5' -CATCGTGGAGAAGGCTCCTA -3'
rev 5' -ATACAGCTGGCCCATGGTAG-3'

Wipi2 fwd 5' -TGCTGGTAGGAGCATCAGATGG-3'
rev 5' -TCACTGGTCGTCTCCATACTGC -3'

RNA-sequencing analysis

Total RNAs were extracted from WT and *Phf20*^{-/-} MEFs with or without glucose starvation, respectively. Then, RNA-seq libraries were produced using Illumina's TruSeq Stranded mRNA LT Sample Prep Kit. After paired-end sequencing of the RNA-seq libraries, adapters and reads with low quality were filtered out by Trimmomatic (v0.36) (Bolger et al., 2014). Then, the trimmed reads were aligned onto the mm10 genome reference using STAR (v2.5.3a) (Dobin et al., 2013), and Transcripts Per Million (TPM) per gene was calculated by RSEM (v1.3.0) (Li and Dewey, 2011). The TPM values were log2-transformed for downstream analyses such as hierarchical clustering, *k*-means clustering and functional analysis. *k*-means clustering was performed to identify the genes regulated by PHF20, and DAVID (v6.8) (Huang da et al., 2009) was utilized for gene ontology. For Gene Set Enrichment Analysis (GSEA) (v 4.0.3) (Subramanian et al., 2005), mm10

annotated protein coding genes were mapped to human protein coding genes using biomaRt (v2.40.5) (Smedley et al., 2009) in R. Phenotype label was assigned as 1:3:1:1 for WT MEFs normal condition: WT MEFs glucose starvation: *Phf20*^{-/-} MEFs normal condition: *Phf20*^{-/-} MEFs glucose starvation, and genes were ranked by the Pearson correlation coefficient. Finally, C2 and C5 gene sets in MSigDB (molecular signatures database) (v7.0) (Liberzon et al., 2015; Liberzon et al., 2011) of the Broad Institute were used for the enrichment score.

Assay for transposase-accessible chromatin using sequencing (ATAC)-sequencing analysis

ATAC-seq libraries were prepared for sequencing using Illumina Tagment DNA TDE1 Enzyme and Buffer Kits (#20034197, Illumina, San Diego, CA, USA) and paired-end sequencing was performed by Illumina platform. Then, paired-end reads were aligned onto mm10 using Burrows-Wheeler Alignment tool (BWA) (v0.7.12) (Li and Durbin, 2009) and peak calling was conducted by Model-based Analysis for ChIP-Seq (MACS) (v2.1.2) (Zhang et al., 2008). For hierarchical clustering based on the peak intensities, the significant peaks were selected with a cut-off false discovery rate (FDR) 0.01 for each sample then merged across the samples. Reads per peak, as an intensity, was counted using BEDTools (v2.25.0) (Quinlan and Hall, 2010). To identify differentially opening peaks (DOPs)

between samples, DESeq2 (v1.26.0) (Love et al., 2014) was applied for the intensities. For average profile of DOPs, normalized read counts centered on peak summits were calculated and plotted by deepTools2 (v3.1.1) (Ramirez et al., 2016)

CHAPTER III

**PHF20 activates autophagy enhancers via the recognition
of H3K36me2 and the recruitment of mixed lineage
leukemia 3/4 (MLL3/4) complex**

III-1. Summary

From previous data, I found that PHF20 deficiency causes decreased autophagy gene expression under glucose starvation. Moreover, PHF20 affects chromatin structure exchange under glucose starvation.

Here, I investigated detailed mechanism of regulation of autophagy genes by PHF20. First, I found that H3K36me2 was enriched in PHF20 dependent chromHMM states. To test possibility that PHF20 directly recognizes H3K36me2, I used *in vitro* biochemical assays including histone peptide binding array and individual peptide binding assay. Results showed that PHF20 bound H3K36me2 via its Tudor domain. Moreover, H3K36me2 binding affinity of PHF20 Tudor domain affected recruitment of PHF20 to the target chromatin regions. After that, I conducted ChIP-sequencing with antibodies for histone markers to check the alteration of epigenetic regulation. From the results, I found that PHF20 depletion caused H3K4me1 and H3K4me2, which were well-known histone markers for active enhancer, to be decreased in PHF20 dependently opened chromatin regions. Furthermore, I found that PHF20 specifically bound MLL3/4 complex and recruit MLL3/4 complex to target enhancer. Recruited MLL3/4 complex induced H3K4me1/2 and activated target enhancers.

These data suggest novel regulatory mechanism of autophagy gene regulation. Especially, the importance of epigenetic regulation and enhancer activity is highlighted. As an epigenetic reader molecule, the function of PHF20 is extended by the investigation of novel binding target, H3K36me2.

III-2. Introduction

Epigenetic regulation of gene expression

In biology, epigenetic regulation means the regulation of gene expression without exchange in DNA sequence. By epigenetic regulation, cells response to extracellular or environmental stimulus and represent phenotypical changes mediated by altered gene expression.

While which biomolecular mechanism mediate epigenetic regulation is not completely understood yet, epigenetic regulation is regarded to consist of three major machinery, DNA methylation, RNA based mechanism and histone modification. In eukaryotes, DNA methylation occurs at CpG sites, exchanging cytosine to 5-methylcytosine. In many case, CpG sites are clustered at 5' regulatory region of genes which called 'CpG island'. When DNA methylation occurs at CpG islands, it induces exchange of chromatin structure through interaction with histone molecules in nucleosome, and affects gene expression. RNA based mechanisms include RNA interference mediated by microRNA, covalent modifications on mRNA and intrinsic functions of long non-coding RNAs (lncRNAs). microRNA and mRNA modification mainly affect to stability or translational efficiency of target transcripts. lncRNAs are known to have its functional activity which are closely correlated with general transcription machinery, or sometimes have its own enzymatic activities. As discovered recently, RNA based mechanisms are not fully understood yet and have much aspects to be elucidated.

Histone modification, another component of epigenetic regulation, gives most variety of

regulatory layer. There are various covalent modifications which can be attached to histone tail; methylation, acetylation, phosphorylation, ubiquitination, sumoylation and glycosylation etc. Moreover, same modification can have different effect depending on the specific amino acid site on histone tail. For example, tri-methylation on Lysin 4 of histone H3 (H3K4me3) is the representative marker of active promoter, while same modification on Lysin 9 of histone H3 (H3K9me3) is mostly enriched in heterochromatin region. Additionally, various histone modifications are orchestrated in combination to specify feature of genome region. Mono-methylated histone H3K4 alone usually marks poised enhancer regions and fully activated enhancers have both H3K4me1 and H3K27Ac. Because histone modifications play an important role in epigenetic gene regulation, they have to be tightly regulated by intercellular signaling cascades.

Through epigenetic regulation, cells can response to extracellular stimulus and survive in various environmental situations. Therefore, investigating epigenetic regulation is a key for understanding the biological physiology.

III-3. Results

PHF20 recognizes H3K36me2 via its Tudor domain

Since the PHF20-dependent chromatin states show a high level of H3K36 methylation as determined by the chromHMM analysis (Figure III-1), I tested the possibility that PHF20 is responsible for chromatin opening at the H3K36me-enriched regions during autophagy. For this, I first examined whether PHF20 recognizes H3K36 methylation directly. Crystal structure of PHF20 predicted that the Tudor domain of PHF20 has a potential for binding di-methylated histone substrates including H3K36me2 (Adams-Cioaba et al., 2012). Moreover, the comparison of the 3D structure of the PHF20 Tudor domain with that of H3K36me2-bound PHF1 Tudor domain from structural modeling allowed us to predict that the PHF20 Tudor domain possesses an aromatic cage structure to be able to accommodate H3K36me2 binding as in the case of PHF1 Tudor domain (Cai et al., 2013).

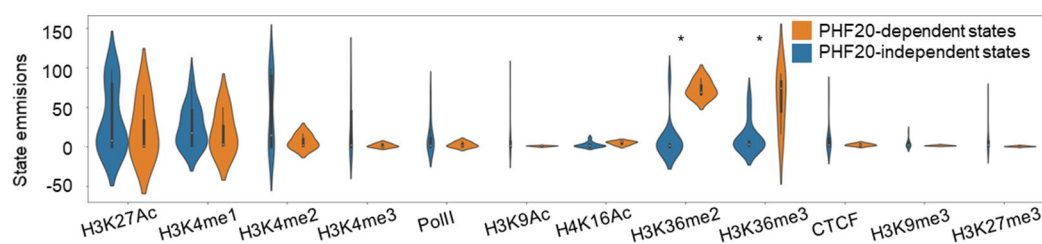


Figure III-1. PHF20 dependent chromHMM states correlate with H3K36 methylation

Relative H3K36me2 ChIP-seq peak intensity of PHF20-dependent (states 6 and 8) and PHF20-independent states in chromHMM.

Therefore, I tested the binding affinity of GST-PHF20 Tudor 1 and 2 domains (Tudor 1&2) to various histone modifications using an *in vitro* histone peptide binding array (Figure III-2A). The peptide binding array revealed specific binding of PHF20 Tudor 1&2 to H3K36me2 as well as other di-methylated lysine peptides (Figure III-2B). Next, I performed an *in vitro* peptide binding assay to examine the binding affinity of GST-PHF20 Tudor 1&2 using WT and mutant W97A; the mutant W97A carries a mutation corresponding to a core aromatic residue to block substrate binding to H3K36me2. GST-PHF20 Tudor 1&2 of WT protein, but not W97A mutant protein, selectively bound the H3K36me2 peptide (Figure III-2C).

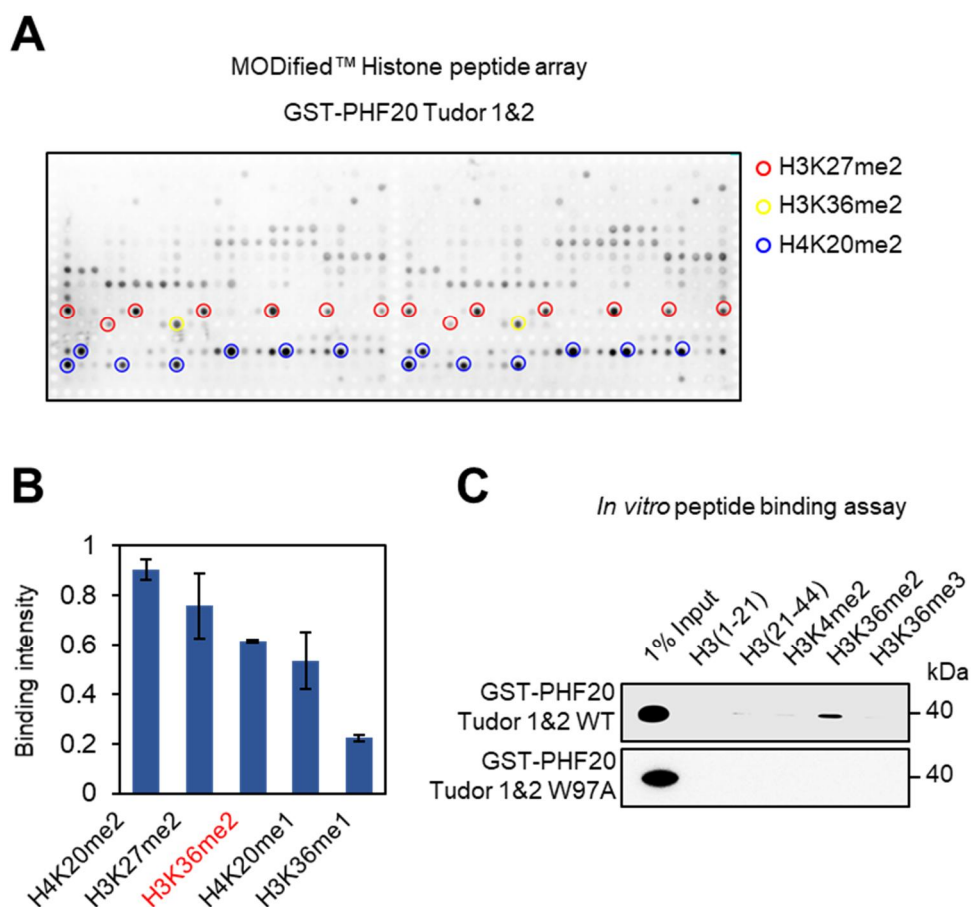


Figure III-2. PHF20 Tudor domain binds H3K36me2

(A) Screening for histone peptide binding of PHF20 Tudor 1 and 2 domains (Tudor 1&2) with MODified™ Histone Peptide Array. GST-PHF20 Tudor 1&2 construct was detected with GST antibody. Histone peptides with significant binding intensity are indicated with red, yellow, and blue circles. Each dot indicated with the color contains the following histone peptides. red:H3K27me2, yellow:H3K36me2, and blue:H4K20me2. (B) Top five histone peptides with the highest binding intensity. Binding intensity was calculated with MODified™ Histone Peptide Array analysis program. (C) *In vitro* peptide binding assay using GST-PHF20 Tudor 1&2 of WT and W97A constructs was performed, followed by immunoblot analysis with anti-GST antibody.

PHF20 recognizes H3K36me2 via its Tudor domain

To test the effect of H3K36me2 binding affinity on the recruitment of PHF20, I conducted the CUT & RUN assay, a chromatin immunocleavage assay with a primary antibody and micrococcal nuclease conjugated with protein A (pA-MN) (Hainer and Fazzio, 2019; Meers et al., 2019), with Flag-PHF20 WT and Δ Tudor mutant (Figure III-3). While the binding of PHF20 WT on the target site increased upon glucose starvation, the Δ Tudor mutant which cannot bind H3K36me2 failed to show increased recruitment upon glucose starvation (Figure III-4).

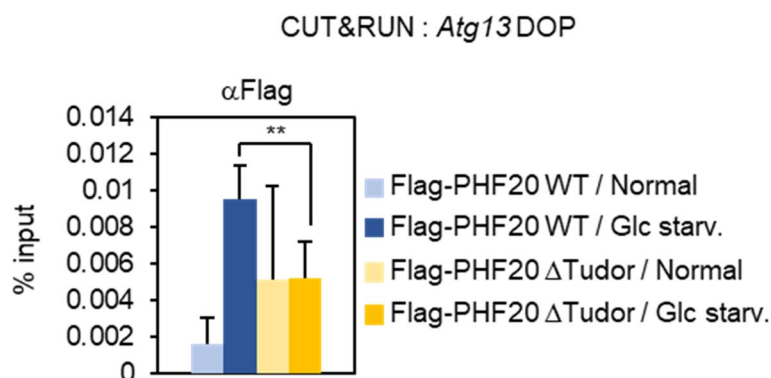


Figure III-3. PHF20 is recruited to target region by Tudor domain

CUT&RUN assay of Flag-tagged PHF20 constructs on *Atg13* DOP region.

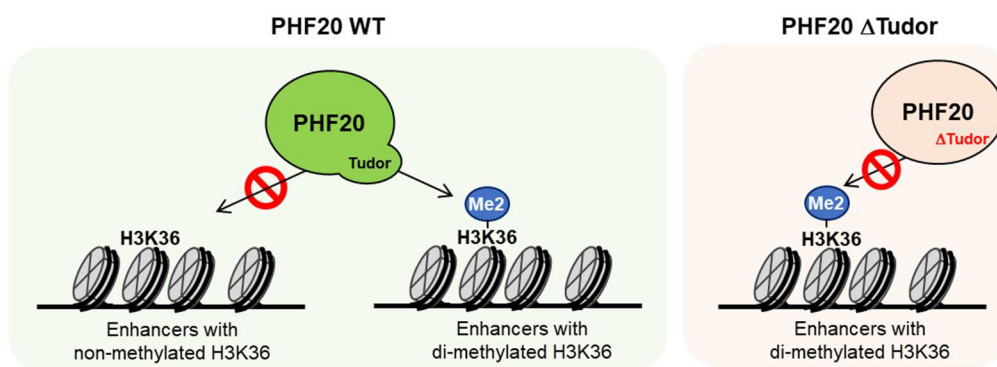


Figure III-4. PHF20 is recruited to target region via recognition of H3K36me2 by Tudor domain

Schematic model for H3K36me2 recognition of PHF20 WT and Tudor domain deletion mutant.

***Phf20* deletion reduces active enhancer markers on its target DOPs.**

Since the chromHMM showed that PHF20-dependent DOPs are localized in non-promoter regions, including an H3K4me-enriched enhancer state (state 8: Enhancer region as shown in Figure II-11), I hypothesized that PHF20 is required for the activation of *cis*-regulatory elements to upregulate autophagy-related genes upon glucose starvation. To test this hypothesis, I performed ChIP-seq for H3K4me1 and H3K4me2, which are known to be closely linked to active *cis*-regulatory elements. Average profiling and read density heatmaps around the peak center revealed that the levels of both H3K4me1 and H3K4me2 increased on PHF20 dependently opened chromatin regions in WT MEFs, but not in *Phf20*^{-/-} MEFs upon glucose starvation (Figure III-5A and 5B).

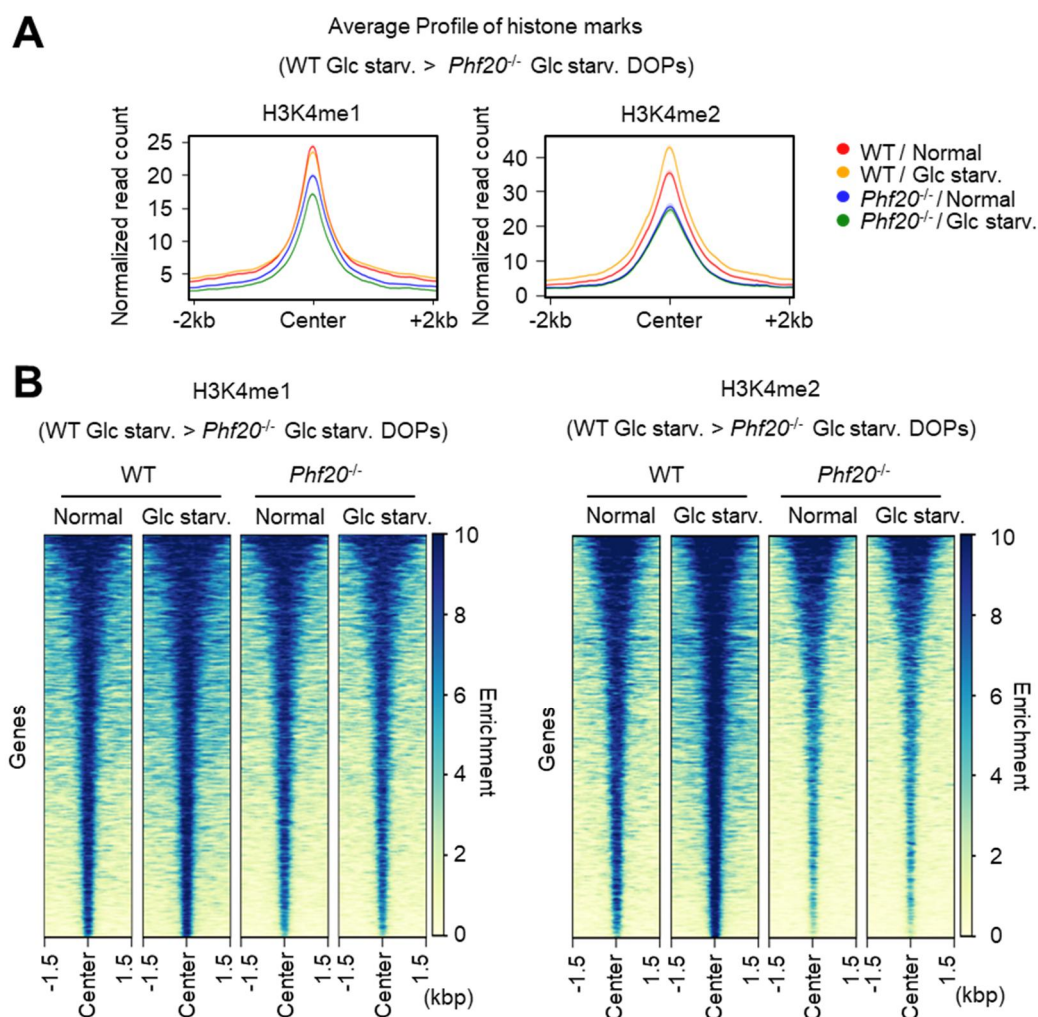


Figure III-5. *Phf20* deletion reduces active enhancer markers on its target DOPs.

(A) Average profiles of H3K4me1 and H3K4me2 signals in WT Glc starv. > *Phf20*^{-/-} Glc starv. DOPs for each condition. (B) Read density heatmaps around peak center of H3K4me1 and H3K4me2 signals in WT Glc starv. > *Phf20*^{-/-} Glc starv. DOPs for each condition.

In particular, the DOPs near the *Supt5*, *Ulk1*, and *Atg13* loci showed marked chromatin opening during autophagy, along with H3K4me1 and H3K4me2 enrichment in WT, but not in *Phf20*^{-/-} MEFs (Figure 4C). Moreover, these three DOPs are closely located to the state 8 enhancer region of chromHMM which shows a PHF20-dependent opening pattern.

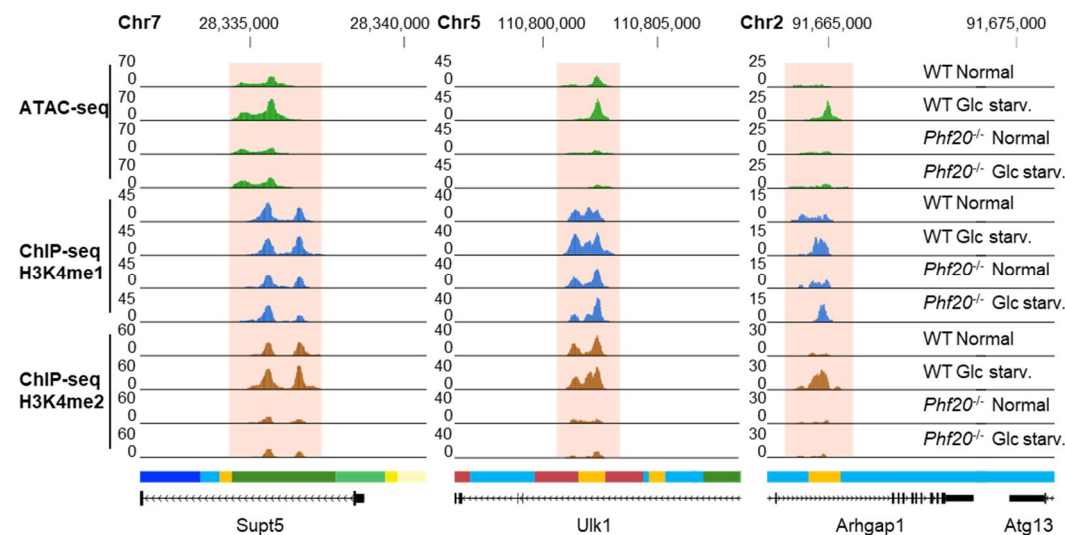


Figure III-6 *Phf20* deletion reduces active enhancer markers on its target DOPs closely located to autophagy related genes.

UCSC Genome Browser (GB) tracks of ATAC-seq signal (green), ChIP-seq signals for H3K4me1 (blue) and H3K4me2 (darkbrown), and chromHMM chromatin states around the DOPs of *Supt5*, *Ulk1* and *Atg13*. Y-axis represents normalized read counts.

PHF20 interacts with MLL3/4 complex

I tried to find out the effector molecules that directly activate the H3K36me2-enriched enhancer regions, given that PHF20 has no enzymatic activity. Since the MLL complexes are well-known methyltransferase complexes for both H3K4me1 and H3K4me2 (Dou et al., 2005; Jeong et al., 2014; Milne et al., 2002; Shilatifard, 2012; Smith et al., 2011), I examined the interaction between PHF20 and MLL components including WDR5 and RbBP5. Co-immunoprecipitation assay revealed that WDR5 and RbBP5 showed comparable binding to PHF20 under glucose starvation (Figure III-7A). Moreover, PHF20 interacted with KDM6A/UTX, a specific component of MLL3/4 complex, but not with Menin, a specific component of MLL1/2 complex, indicating that PHF20 has a binding preference for MLL3/4 complex (Figure III-7B). Because MLL3/4 complex are known to play an important role in establishing H3K4me1 on enhancer, this result supports that PHF20 is mainly responsible for enhancer activation upon glucose starvation.

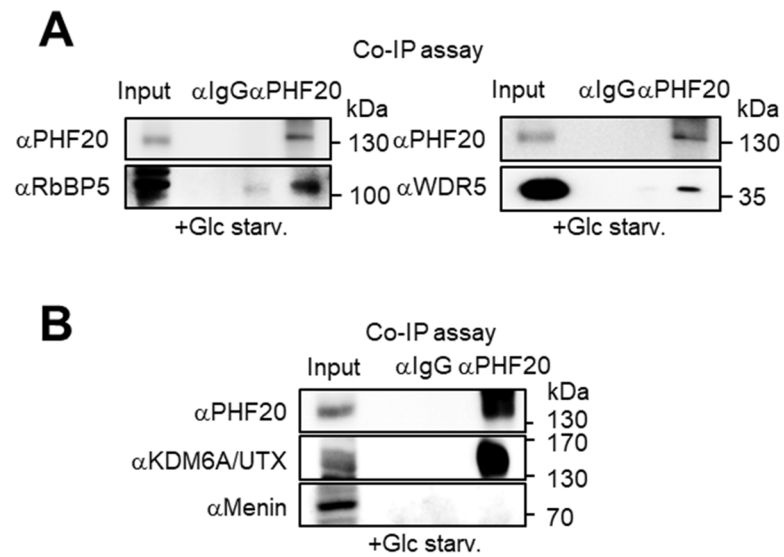


Figure III-7. PHF20 binds MLL3/4 complex

(**A and B**) Co-immunoprecipitation assay of endogenous PHF20 with WRAD components including WDR5 and RbBP5 (**A**) or MLL subtype specific components exemplified by Menin (MLL1/2 complex-specific) and KDM6A/UTX (MLL3/4 complex-specific) (**B**) under glucose starvation.

PHF20 activates enhancers via the recruitment of mixed lineage leukemia 3/4 (MLL3/4) complex

To test whether PHF20 recruits the MLL3/4 complex to H3K36me2-enriched target sites under glucose starvation, I performed ChIP assay and checked the recruitment of WDR5 to PHF20-dependent DOPs (Figure III-8). WDR5 was recruited to the target DOPs under glucose starvation in WT MEFs, but not in *Phf20*^{-/-} MEFs. Moreover, the transcription of eRNA, which is closely correlated with enhancer activity (Li et al., 2013; Wang et al., 2011), increased under glucose starvation in WT MEFs, but not in *Phf20*^{-/-} MEFs (Figure III-9).

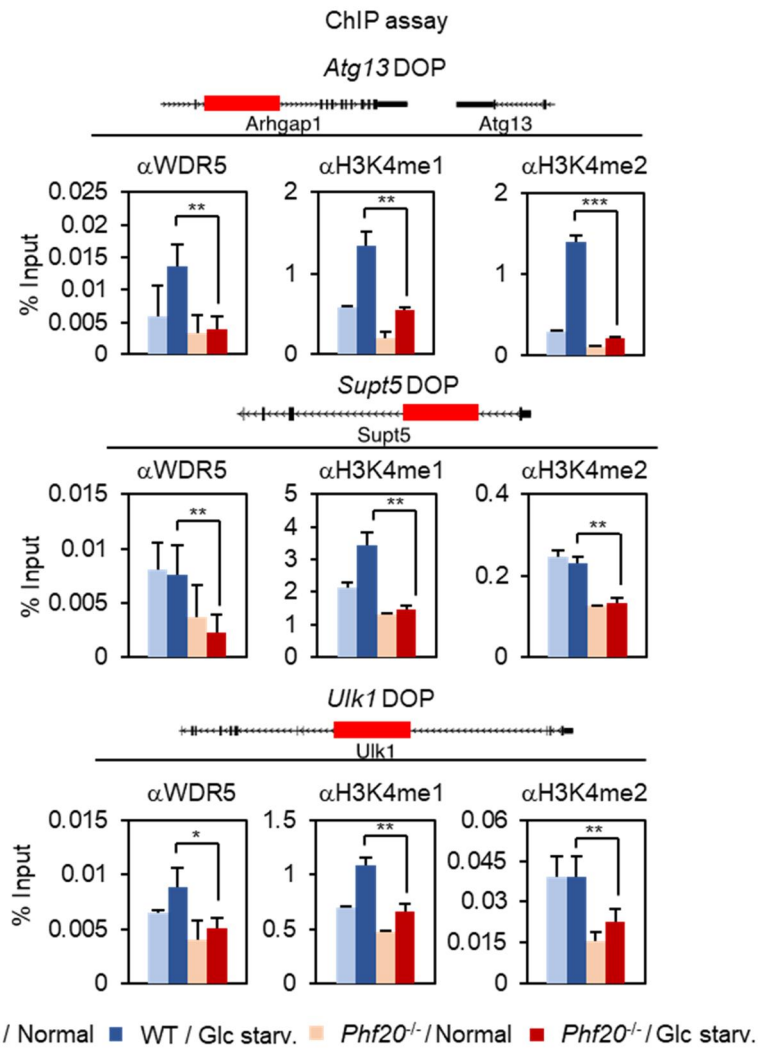


Figure III-8. PHF20 recruits MLL3/4 complex to the target enhancers

Chromatin immunoprecipitation (ChIP) assay was detected by individual qRT-PCR with primers for *Atg13*, *Ulk1* and *Supt5* DOP regions. Bars, mean \pm SEM; *** $p < 0.001$, ** $p < 0.01$. Statistical analysis using two-tailed t-test.

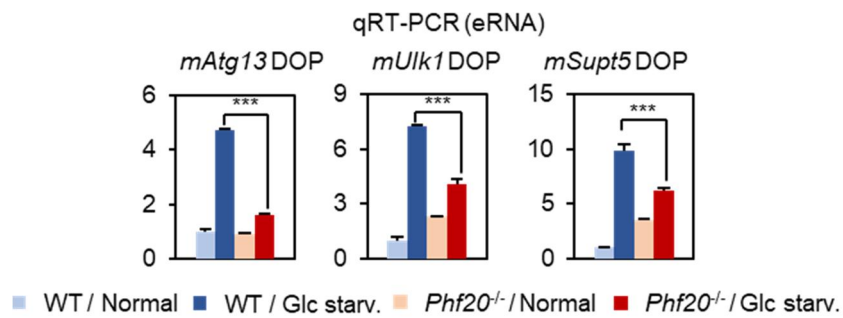


Figure III-9. Expression of eRNA on target enhancer is induced by PHF20

qRT-PCR for expression of enhancer RNA (eRNA) on Atg13, Ulk1 and Supt5 DOP regions. Bars, mean \pm SEM; *** $p < 0.001$. Statistical analysis using two-tailed t-test.

Next, I tested the effect of PHF20-dependent enhancer activity on its target gene expression using CRISPRi. I used a fusion protein of the enzymatically inactive dCas9 and Krüppel-associated box (KRAB) repressor (dCas9-KRAB) to repress the target enhancer regions (Thakore et al., 2015). Inhibition of the enhancer region by CRISPRi led to a decrease in target gene expression exemplified by Atg13 and Ulk1 without affecting promoter activity (Figure III-10A and 10B).

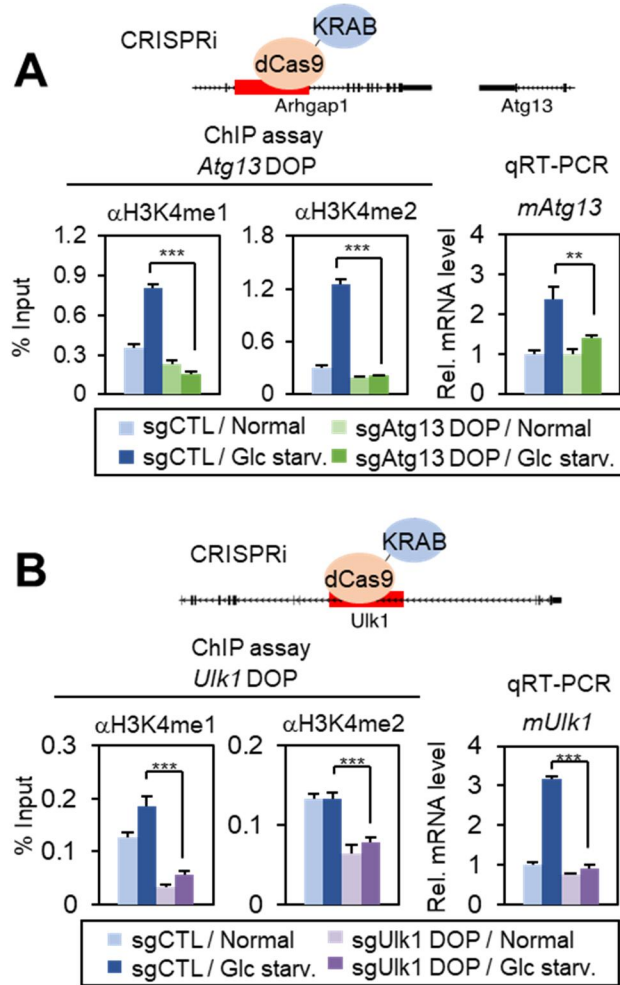


Figure III-10. Activity of PHF20 dependent DOP affects to expression of autophagy related genes

(A) qRT-PCR for ChIP assay with histone H3K4me1 and H3K4me2 antibodies on Atg13 DOP region (left panel) and qRT-PCR of Atg13 mRNA (right panel). sgAtg13 cell line was generated by CRISPRi system with sgRNA targeting Atg13 DOP region. Bars, mean \pm SEM; *** $p < 0.001$, ** $p < 0.01$. Statistical analysis using two-tailed t-test. (B) qRT-PCR analysis after ChIP assay with H3K4me1 and H3K4me2 antibodies on Ulk1 DOP region (left panel) and qRT-PCR of Ulk1 mRNA (right panel). sgUlk1 cell line was generated by CRISPRi system with sgRNA targeting Ulk1 DOP region. Bars, mean \pm SEM; *** $p < 0.001$. Statistical analysis using two-tailed t-test.

At last, I confirmed the PHF20 dependent promoter-enhancer looping with chromosome conformation capture (3C) assay (Figure III-11A-11C). The looping between the PHF20 dependent target gene promoters and DOP regions increased under glucose starvation in WT MEFs, but not in *Phf20*^{-/-} MEFs. Taken together, our data indicate that PHF20 increases the expression of autophagy genes via enhancer activation by recruiting the MLL3/4 complex to the target DOPs under glucose starvation (Figure III-12).

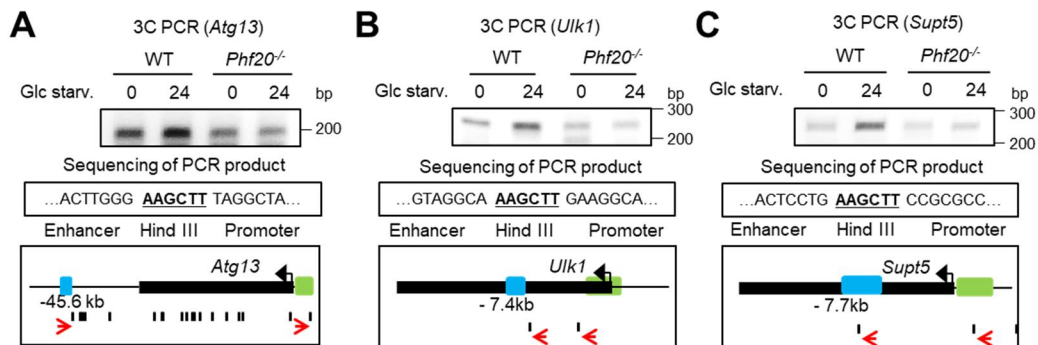


Figure III-11. Enhancer-promoter looping occurs between PHF20 dependent DOPs and promoters of autophagy related genes

(A-C) Chromosome conformation capture (3C) assay on promoter-enhancer region of PHF20 target genes including *Atg13* (A), *Ulk1* (B) and *Supt5* (C). PCR products were detected by DNA gel electrophoresis. DNA sequencing results were indicated (middle box). The models describe promoters (green blocks) with possible enhancer elements (blue blocks). Black lines represent HindIII restriction sites. Red arrows represent the site and the direction of primers used in PCR (bottom box).

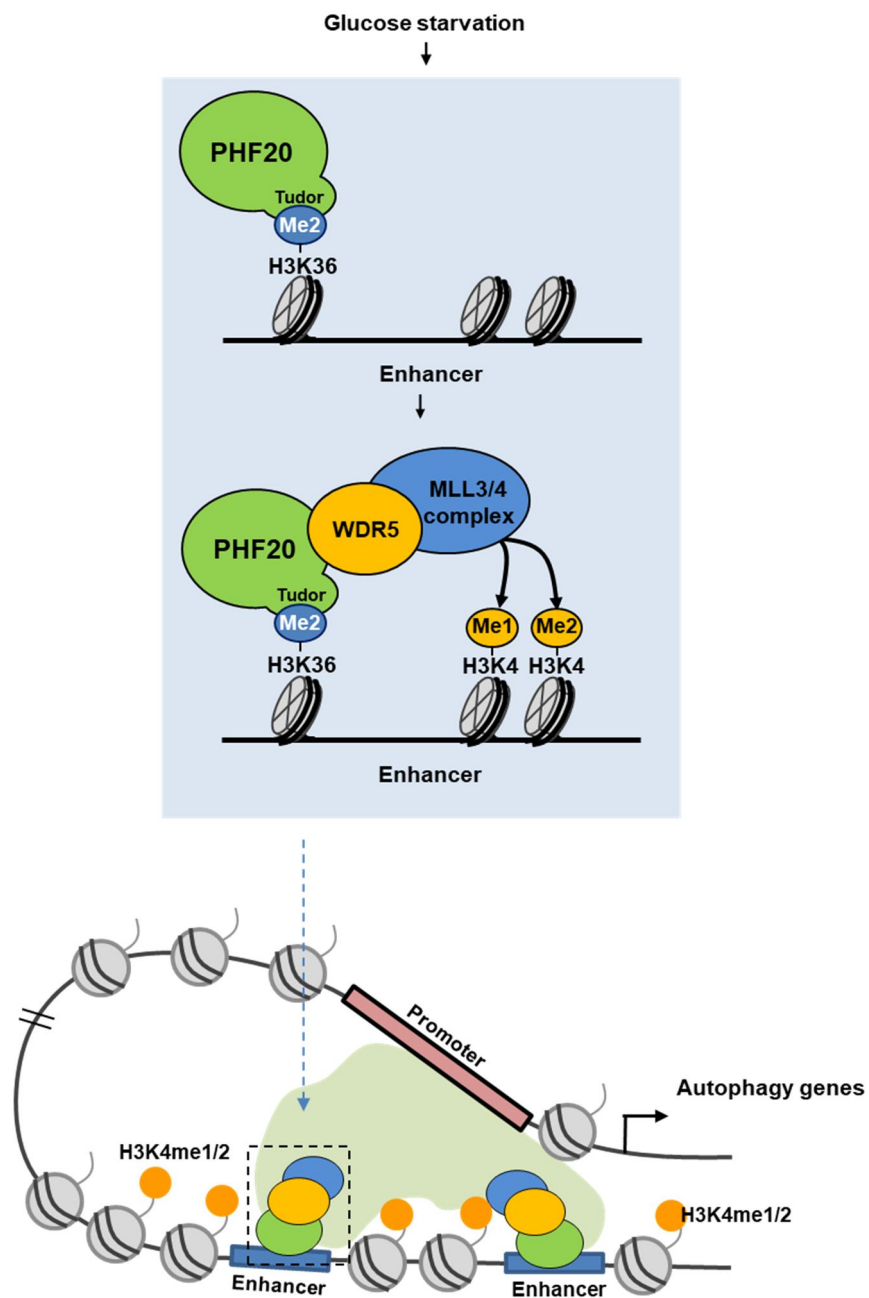


Figure III-12. PHF20 is crucial for epigenetic regulation of autophagy via H3K36me2-dependent enhancer activation.

III-4. Discussion

Genome-wide analyses and molecular mechanistic studies revealed that PHF20 functions as a versatile platform for recruiting MLL3/4 methyltransferase complexes with increased histone H3K4 methylation and the subsequent activation of autophagy genes. Intriguingly, glucose starvation-induced PHF20-MLL3/4 complex can work in the distal regions and activate autophagy genes through enhancer activation. Histone H3K36me2 in enhancer regions is recognized by PHF20 through the Tudor 1 and 2 domains and this recognition is required for the activation of the transcription of autophagy genes, leading to the continued autophagic flux. Given that PHF20 plays an important role in stress-induced autophagy, connections between H3K36me2-enriched regions and enhancer activation by PHF20 reveal a new way in which cells cope with various harmful conditions.

As neither PHF20 protein level nor H3K36me2 level is increased by glucose starvation, we speculate that certain signal-induced post-translational modifications of PHF20 may contribute to the increased recruitment of PHF20 to H3K36me2-enriched chromatin regions during starvation-induced autophagy. Another possibility is that certain transcription factors and coregulators function to facilitate the enhanced binding of PHF20 to H3K36me2-enriched target sites. Since deletion of the Tudor domain of PHF20 led to the failure of PHF20 recruitment to the H3K36me2-enriched region, certain post-translational modifications of PHF20 may occur on the Tudor domain or nearby regions to make it effective for accommodating H3K36me2 binding. Moreover, we found that PHF20 Tudor domain also showed comparable binding to H4K20me2 and H3K27me2 from *in vitro*

peptide binding array. In this study, we only focused on H3K36me2 to further studies, although it is possible that H4K20me2 or H3K27me2 might have functions to induce the binding of PHF20 to the target sites.

SET1 family methyltransferases including the MLL family proteins should be associated with WRAD components—which comprise WDR5, RbBP5, Ash2L and DPY-30—for their complete activation (Ernst and Vakoc, 2012; Miller *et al.*, 2001). WRAD induces the allosteric activation of methyltransferases or recruits methyltransferases to the appropriate target sites (Bryk *et al.*, 2010; Patel *et al.*, 2009; Patel *et al.*, 2011; Steward *et al.*, 2006). Since the MLL complex is responsible for all three types of H3K4 methylations, each subtype of MLL complex possesses distinct enzymatic activity toward its substrate; MLL1/2 is a major methyltransferase for H3K4me3 on promoters (Hu *et al.*, 2013; Wang *et al.*, 2009), while MLL3/4 is responsible for the accumulation of H3K4me1 on active enhancers (Herz *et al.*, 2012; Lee *et al.*, 2013; Liu *et al.*, 2019). Therefore, the genomic site where each subtype of the MLL complex is recruited under specific conditions should be tightly regulated. Our finding regarding the recruitment of WDR5 and RbBP5 by PHF20 to the target enhancer site suggests that PHF20 plays an important role in inducing H3K4 methylation via the MLL complex. Especially, our immunoprecipitation data shows that PHF20 has a binding preference to MLL3/4 complex compared to MLL1/2 complex. Therefore, our data suggest that PHF20 with H3K36me2 binding activity might contribute to the regulation of the subtype-specific target decision between the MLL complexes, depending on the upstream signals.

The epigenetic and transcriptional control of autophagy is mainly triggered by upstream

signaling cascades, and then regulated by epigenetic enzymes in the nucleus. Histone modifications and epigenetic enzymes are linked to the transcriptional regulation of autophagy depending upstream signals. We have previously identified CARM1 arginine methyltransferase as an essential regulator of both TFEB and FOXO transcription factors. CARM1 directly functions as a coactivator for TFEB with increased H3R17 methylation. CARM1 also has a nonhistone substrate, Pontin, as well as a histone substrate, H3R17me2; methylated Pontin functions as a coactivator of FOXO, with increased H4 acetylation by the Tip60 coactivator (Yu et al., 2020). Compared to the specific PHF20 binding to an enhancer region, methylated Pontin can bind both the distal DNA region and the promoter region via FOXO3a binding. Although further studies are needed to understand how PHF20-dependent enhancers and methylated Pontin-FOXO3a-dependent enhancers are orchestrated to work with promoters to regulate autophagy genes upon glucose starvation, our study suggests the possibility that there exist various ways of enhancer activation via a distinct signaling axis. We speculate that pharmacological manipulation would be helpful in controlling autophagy as well as autophagy-related diseases by selectively blocking transcription factors, coregulators, and various signaling axes.

III-5. Materials and Methods

Purification of GST-fusion proteins and *in vitro* peptide binding assay

GST-tagged PHF20 Tudor 1 and 2 domains (Tudor 1&2, 1-147 a.a) of WT or W97A mutant constructs were cloned in pGEX-4T-1 vector and were transformed in Rosetta *E. coli* strain. The protein was purified with glutathione beads (GE17-0756-01, GE Healthcare, Chicago, IL, USA) and eluted with elution buffer (50 mM Tris-HCl [pH 7.5], 100 mM NaCl, 10 mM reduced glutathione, and 1 mM DTT supplemented with 1X complete protease inhibitor). For *in vitro* peptide binding assay, 2 µg of WT and W97A purified proteins were incubated overnight with 1 µg of biotin-labeled protein peptides in the 300 µl of binding buffer (50 mM Tris-HCl [pH 7.5], 200 mM NaCl, and 0.05 % NP-40). Then, 30 µl of streptavidin sepharose beads were added to each tube and incubated for 1 hr. After binding, beads were washed 4 times with binding buffer and samples were boiled with 30 µl of SDS sampling buffer.

***In vitro* histone peptide binding array**

In vitro histone peptide binding array was performed with MODified™ Histone Peptide Array Kit (13001, Active Motif, Carlsbad, CA, USA) following manufacturer's protocol.

In brief, array kit was blocked with 5 % milk in TTBS (10 mM Tris-HCl [pH 7.5] , 150 mM NaCl, and 0.05 % Tween-20) at 4 °C overnight. After that, the kit was incubated with purified GST-PHF20 Tudor 1&2 WT protein in binding buffer (20 mM HEPES [pH 7.9], 100 mM KCl, 1 mM EDTA, 10 % glycerol, and 0.1 mM DTT) for 1 hr. Then, primary GST antibody and secondary antibody were treated and bound GST proteins were detected with ECL solution.

Chromatin immunoprecipitation (ChIP) assay

Before crosslinking, cells were washed three times with cold PBS to remove amine-containing proteins from cells and media. Then, ethylene glycolbis(succinimidylsuccinate) (EGS) was treated to the cell for final concentration of 2 mM at 20-22 °C. After 20 minutes, 1 % formaldehyde was added and cells were incubated for 10 minutes. After glycine quenching, cells were harvested and resuspended with ChIP lysis buffer containing 50 mM Tris-HCl [pH 8.1], 10 mM EDTA, 1 % SDS, and protease inhibitor cocktail. DNA was fragmented with sonication until average size reaches 250 bp. Dilution buffer containing 20 mM Tris-HCl [pH 8.1], 150 mM NaCl, 2 mM EDTA, and 1 % Triton X-100 were added to chromatin extract with a volume of ten times. Diluted samples were subjected to immunoprecipitation with assigned antibodies overnight at 4 °C. Then, 40 µl of Protein A/G sepharose beads were added to capture immunocomplexes. After 2 hr of incubation at

4 °C, beads were washed with TSE I buffer (20 mM Tris–HCl [pH 8.1], 0.1 % SDS, 1 % Triton X-100, 2 mM EDTA, and 150 mM NaCl), TSE II buffer (20 mM Tris–HCl [pH 8.1], 0.1 % SDS, 1 % Triton X-100, 2 mM EDTA, and 500 mM NaCl), buffer III (10 mM Tris–HCl [pH 8.1], 0.25 M LiCl, 1 % NP-40, 1 % deoxycholate, and 1 mM EDTA), three times TE buffer (10 mM Tris-HCl [pH 8.0] and 1 mM EDTA). Immunocomplex was eluted from beads by incubation with elution buffer (1 % SDS and 0.1 M NaHCO₃) for 2 hr and the elute was reverse crosslinked by overnight incubation at 65 °C. RNAs and proteins in sample were digested with RNase and protease K. Final samples and matched input samples were analyzed with quantitative-RT PCR or subjected to construct sequencing libraries. The following primers are used for qRT-PCR.

<i>Atg13</i> DOP	fwd	5' -CTCTGTGTGCCCTGTTTT-3'
	rev	5' -GAGCTACCTCCAAGCACACA-3'
<i>Ulk1</i> DOP	fwd	5'-ATAGGATCCCAGCTCTCCAC-3'
	rev	5'-CTAGAGCCTTGGCACCTTCT-3'
<i>Supt5</i> DOP	fwd	5'-TGCTGGGATTAAAGGCATGC-3'
	rev	5'-CCTGATGTCCTGGGATCTGT-3'

Chromatin immunoprecipitation (ChIP)-sequencing analysis

Paired-end reads were aligned onto the mm10 reference genome using BWA (v0.7.12), and MACS (v2.1.2) was utilized to identify significant peaks with cut-offs of false discovery rate (FDR) 0.01 and signal value 5.

CUT&RUN assay

CUT&RUN assay kit (#86652, Cell Signaling) was used following manufacturer's instruction. In brief, collected cells were washed with wash buffer and permeabilized with Digitonin solution. Then, cells were bound to Concanavalin A magnetic beads and incubated with antibody overnight at 4 °C. Next, pAG-MNase was treated to fragment DNA where target protein is attached. DNA extract was purified with DNA Purification Buffers and Spin Columns (#14209, Cell signaling) and subjected to qRT-PCR. The following primers are used for qRT-PCR.

Atg13 DOP fwd 5' -ACTGTGCTTCCACTGGCTCT-3'

rev 5' -CAGTGGGGAAAGCCAAGTCT-3'

Chromosome conformation capture (3C) assay

The 3C assays were performed as modified version of previous methods (Hagege et al., 2007; Naumova et al., 2012). In brief, 1×10^7 cells were crosslinked in 1 % formaldehyde/media for 10 min at 20-22 °C. After crosslinking step, glycine was added to a final concentration of 0.125 M and incubated for 10 min. After washing with DPBS for 2 times, cells were harvested and lysed with Buffer I (10 mM HEPES [pH 6.5], 0.25 % Triton X-100, 10 mM EDTA, and 0.5 mM EGTA) and Buffer II (10 mM HEPES [pH 6.5], 200 mM NaCl, 1 mM EDTA, and 0.5 EGTA) at 4°C for 5 min, respectively. Cells were additionally lysed with lysis buffer (10 mM Tris-HCl [pH 7.5], 10 mM NaCl, 0.2 % NP-40, and 1X complete protease inhibitor). After centrifugation, the pelleted nuclei were resuspended with 1.2 X restriction enzyme buffer M (Takara, Kusatsu, Japan) with 0.3 % (w/v) SDS and incubated at 37 °C while shaking at 900 r.p.m. Triton X-100 was added to a final concentration of 2 % (v/v) and incubated at 37 °C while shaking at 900 r.p.m. 400U of restriction enzyme HindIII (1060BH, Takara) was added and incubated overnight at 37 °C while shaking at 900 r.p.m. for chromatin digestion. For restriction enzyme inactivation, SDS was added to a final concentration of 1.6 % and samples were incubated for 20 minutes at 65 °C while shaking at 900 r.p.m. Before ligation, 1.15X filtered ligation buffer (66 mM Tris-HCl [pH 7.5], 5 mM DTT, 5 mM MgCl₂, and 1 mM ATP) and 1 % Triton X-100 was added and were incubated for 1 hr at 37 °C while shaking gently. The

DNA was ligated by 100U T4 DNA ligase (M053L, Enzymomics) at 16 °C for 4 hr followed by 30 min incubation at 20-22 °C. 300 µg of Protease K (P2308, Sigma-aldrich) was added and the DNA was de-crosslinked at 65 °C overnight. DNA purification was performed by phenol-chloroform extraction and ethanol precipitation. The following PCR program was used: 95 °C for 10 min, followed by 38 cycles of 95 °C for 10 s, 60 °C for 10 s, and 72 °C for 10 s. The following primers were used.

Atg13 promoter fwd (P) 5'-ACTGTTTTGAAAGCGGGTTG-3';

Atg13 enhancer fwd (E) 5'-CGGTTGGTTCCTTGTGAATC-3';

Ulk1 promoter rev (P) 5'-TCCCCACAGTTTTTGGTTTC-3';

Ulk1 enhancer rev (E) 5'-TACCCACAGGGCCATCTTTA-3';

Supt5 promoter rev (P) 5'-GAGCAGGCCCTAAAGTCTC-3';

Supt5 enhancer rev (E) 5'-TGGCTTTTTAAACCGTGAGG-3';

Statistical analysis

All experiments were performed independently at least three times. Prism v5 software (GraphPad) was used for statistical analysis. Student's *t*-test was used for comparison between two groups. Analysis of variance (ANOVA) with post hoc tests was used for

comparison of multiple samples and discrimination of significant relationships. *P*-values less than 0.05 were considered statistically significant.

DATA AVAILABILITY

RNA-seq, ChIP-seq, and ATAC-seq data have been deposited with the Gene Expression Omnibus (GEO) under accession number GSE193393. To characterize chromatin states of MEFs, chromHMM was performed with 12 previously published ChIP-seq data sets (CTCF: GSE36027, H3K27ac: GSE31039, GSE113429, H3K27me3: GSE26099, GSE26657, H3K36me2: GSE160266, H3K36me3: GSE26099, H3K4me1: GSE31039, H3K4me2: GSE90893, H3K4me3: GSE31039, GSE26657, H3K9ac: GSM2417089, H3K9me3: GSE26657, H4K16ac: GSE97459, PolIII: GSE36027)

CHAPTER IV

Conclusion

In this study, I report a novel signaling pathway which is critical for the epigenetic control of autophagy. I identify PHF20 as a critical epigenetic reader for autophagy gene expression through enhancer activation via H3K36me2 recognition and that *Phf20* deficiency led to impaired autophagic flux and autophagy gene expression under glucose starvation. Importantly, the recognition of H3K36me2 by PHF20 was highly correlated with increased level of H3K4me1/2 in enhancer by recruiting MLL complex.

Despite the importance of epigenetic regulation on gene expression, its mechanism on autophagy related gene under stress condition was not clearly understood. This study provides novel insight on the importance of epigenetic regulation and histone modification dynamics during autophagy gene expression in starvation-induced autophagy through PHF20 dependent enhancer activating mechanism. Moreover, as PHF20 is an epigenetic reader molecule which plays important roles on histone methyl/acetyltransferase complexes, this study expands the understanding of the functions of epigenetic reader molecule in epigenetic transcription regulation.

To identify the molecular mechanism of PHF20, I conducted various genome-wide sequencing including RNA-seq, ATAC-seq and ChIP-seq. Furthermore, using chromHMM which is computational learning method with 12 different public ChIP-seq data, I defined functional classification of whole genome of mouse embryonic fibroblasts. From combined investigation of various genome-wide data, I suggested guideline for integrative analysis of transcriptome, chromatin structure and epigenetic status.

Because H3K4 methylation by MLL complex is known to be induced by diverse stimuli as well as glucose starvation, PHF20 dependent enhancer activation mechanism is expected

to be applied to other signaling pathways. In many cases, gene expression feature of given cell type or situation is achieved by selective activation of specific enhancers. Given that PHF20 dependent enhancer activation mechanism targets specific enhancers with highly enriched H3K36me2 marker, this mechanism can contribute to establish gene expression pattern in various cellular context including immune response, cellular senescence or tumorigenesis.

As deregulation of the autophagy has a critical impact on the maintenance of homeostasis as well as onset of human diseases, the discovery of epigenetic control of the autophagy will greatly advance our understanding of health and diseases. Especially, PHF20 is expected to be a high-selective therapeutic target for autophagy related human disease because PHF20 dependent autophagy gene expression mechanism is only activated under autophagy inducing signals and it specifically targets selective enhancers with H3K36me2 enriched chromatin status.

This study expands the understanding of epigenetic regulation of gene expression and autophagy induction by glucose starvation. Moreover, this study gives novel insight on clinical approach for autophagy related human diseases.

REFERENCES

- Adams-Cioaba, M.A., Li, Z., Tempel, W., Guo, Y., Bian, C., Li, Y., Lam, R., and Min, J. (2012). Crystal structures of the Tudor domains of human PHF20 reveal novel structural variations on the Royal Family of proteins. *FEBS Lett* 586, 859-865. 10.1016/j.febslet.2012.02.012.
- Alam, H., Gu, B., and Lee, M.G. (2015). Histone methylation modifiers in cellular signaling pathways. *Cell Mol Life Sci* 72, 4577-4592. 10.1007/s00018-015-2023-y.
- Badeaux, A.I., Yang, Y., Cardenas, K., Vemulapalli, V., Chen, K., Kusewitt, D., Richie, E., Li, W., and Bedford, M.T. (2012). Loss of the methyl lysine effector protein PHF20 impacts the expression of genes regulated by the lysine acetyltransferase MOF. *J Biol Chem* 287, 429-437. 10.1074/jbc.M111.271163.
- Baek, S.H., and Kim, K.I. (2017). Epigenetic Control of Autophagy: Nuclear Events Gain More Attention. *Mol Cell* 65, 781-785. 10.1016/j.molcel.2016.12.027.
- Ballare, C., Lange, M., Lapinaite, A., Martin, G.M., Morey, L., Pascual, G., Liefke, R., Simon, B., Shi, Y., Gozani, O., et al. (2012). Phf19 links methylated Lys36 of histone H3 to regulation of Polycomb activity. *Nat Struct Mol Biol* 19, 1257-1265. 10.1038/nsmb.2434.
- Biswas, S., and Rao, C.M. (2018). Epigenetic tools (The Writers, The Readers and The Erasers) and their implications in cancer therapy. *Eur J Pharmacol* 837, 8-24. 10.1016/j.ejphar.2018.08.021.
- Bolger, A.M., Lohse, M., and Usadel, B. (2014). Trimmomatic: a flexible trimmer for

Illumina sequence data. *Bioinformatics* 30, 2114-2120. 10.1093/bioinformatics/btu170.

Bryk, M., Cao, F., Chen, Y., Cierpicki, T., Liu, Y., Basrur, V., Lei, M., and Dou, Y. (2010). An Ash2L/RbBP5 Heterodimer Stimulates the MLL1 Methyltransferase Activity through Coordinated Substrate Interactions with the MLL1 SET Domain. *PLoS ONE* 5. 10.1371/journal.pone.0014102.

Cai, L., Rothbart, S.B., Lu, R., Xu, B., Chen, W.Y., Tripathy, A., Rockowitz, S., Zheng, D., Patel, D.J., Allis, C.D., et al. (2013). An H3K36 methylation-engaging Tudor motif of polycomb-like proteins mediates PRC2 complex targeting. *Mol Cell* 49, 571-582. 10.1016/j.molcel.2012.11.026.

Cai, Y., Jin, J., Swanson, S.K., Cole, M.D., Choi, S.H., Florens, L., Washburn, M.P., Conaway, J.W., and Conaway, R.C. (2010). Subunit composition and substrate specificity of a MOF-containing histone acetyltransferase distinct from the male-specific lethal (MSL) complex. *J Biol Chem* 285, 4268-4272. 10.1074/jbc.C109.087981.

Choi, A.M., Ryter, S.W., and Levine, B. (2013). Autophagy in human health and disease. *N Engl J Med* 368, 651-662. 10.1056/NEJMr1205406.

Cui, G., Park, S., Badeaux, A.I., Kim, D., Lee, J., Thompson, J.R., Yan, F., Kaneko, S., Yuan, Z., Botuyan, M.V., et al. (2012). PHF20 is an effector protein of p53 double lysine methylation that stabilizes and activates p53. *Nat Struct Mol Biol* 19, 916-924. 10.1038/nsmb.2353.

Dobin, A., Davis, C.A., Schlesinger, F., Drenkow, J., Zaleski, C., Jha, S., Batut, P., Chaisson, M., and Gingeras, T.R. (2013). STAR: ultrafast universal RNA-seq aligner. *Bioinformatics* 29, 15-21. 10.1093/bioinformatics/bts635.

- Dou, Y., Milne, T.A., Tackett, A.J., Smith, E.R., Fukuda, A., Wysocka, J., Allis, C.D., Chait, B.T., Hess, J.L., and Roeder, R.G. (2005). Physical association and coordinate function of the H3 K4 methyltransferase MLL1 and the H4 K16 acetyltransferase MOF. *Cell* *121*, 873-885. 10.1016/j.cell.2005.04.031.
- Ernst, J., and Kellis, M. (2012). ChromHMM: automating chromatin-state discovery and characterization. *Nat Methods* *9*, 215-216. 10.1038/nmeth.1906.
- Ernst, J., and Kellis, M. (2017). Chromatin-state discovery and genome annotation with ChromHMM. *Nat Protoc* *12*, 2478-2492. 10.1038/nprot.2017.124.
- Ernst, P., and Vakoc, C.R. (2012). WRAD: enabler of the SET1-family of H3K4 methyltransferases. *Brief Funct Genomics* *11*, 217-226. 10.1093/bfgp/els017.
- Fullgrabe, J., Klionsky, D.J., and Joseph, B. (2014). The return of the nucleus: transcriptional and epigenetic control of autophagy. *Nat Rev Mol Cell Biol* *15*, 65-74. 10.1038/nrm3716.
- Glick, D., Barth, S., and Macleod, K.F. (2010). Autophagy: cellular and molecular mechanisms. *J Pathol* *221*, 3-12. 10.1002/path.2697.
- Greer, E.L., and Shi, Y. (2012). Histone methylation: a dynamic mark in health, disease and inheritance. *Nat Rev Genet* *13*, 343-357. 10.1038/nrg3173.
- Hagege, H., Klous, P., Braem, C., Splinter, E., Dekker, J., Cathala, G., de Laat, W., and Forne, T. (2007). Quantitative analysis of chromosome conformation capture assays (3C-qPCR). *Nat Protoc* *2*, 1722-1733. 10.1038/nprot.2007.243.
- Hainer, S.J., and Fazzio, T.G. (2019). High-Resolution Chromatin Profiling Using CUT&RUN. *Curr Protoc Mol Biol* *126*, e85. 10.1002/cpmb.85.

- Han, X., Gui, B., Xiong, C., Zhao, L., Liang, J., Sun, L., Yang, X., Yu, W., Si, W., Yan, R., et al. (2014). Destabilizing LSD1 by Jade-2 promotes neurogenesis: an antibraking system in neural development. *Mol Cell* 55, 482-494. 10.1016/j.molcel.2014.06.006.
- Herz, H.M., Mohan, M., Garruss, A.S., Liang, K., Takahashi, Y.H., Mickey, K., Voets, O., Verrijzer, C.P., and Shilatifard, A. (2012). Enhancer-associated H3K4 monomethylation by Trithorax-related, the Drosophila homolog of mammalian Mll3/Mll4. *Genes Dev* 26, 2604-2620. 10.1101/gad.201327.112.
- Hu, D., Garruss, A.S., Gao, X., Morgan, M.A., Cook, M., Smith, E.R., and Shilatifard, A. (2013). The Mll2 branch of the COMPASS family regulates bivalent promoters in mouse embryonic stem cells. *Nat Struct Mol Biol* 20, 1093-1097. 10.1038/nsmb.2653.
- Huang da, W., Sherman, B.T., and Lempicki, R.A. (2009). Bioinformatics enrichment tools: paths toward the comprehensive functional analysis of large gene lists. *Nucleic Acids Res* 37, 1-13. 10.1093/nar/gkn923.
- Hyun, K., Jeon, J., Park, K., and Kim, J. (2017). Writing, erasing and reading histone lysine methylations. *Exp Mol Med* 49, e324. 10.1038/emm.2017.11.
- Jeong, K.W., Andreu-Vieyra, C., You, J.S., Jones, P.A., and Stallcup, M.R. (2014). Establishment of active chromatin structure at enhancer elements by mixed-lineage leukemia 1 to initiate estrogen-dependent gene expression. *Nucleic Acids Res* 42, 2245-2256. 10.1093/nar/gkt1236.
- Kim, C.R., Noda, T., Kim, H., Kim, G., Park, S., Na, Y., Oura, S., Shimada, K., Bang, I., Ahn, J.Y., et al. (2020). PHF7 Modulates BRDT Stability and Histone-to-Protamine Exchange during Spermiogenesis. *Cell Rep* 32, 107950. 10.1016/j.celrep.2020.107950.

- Klein, Brianna J., Wang, X., Cui, G., Yuan, C., Botuyan, Maria V., Lin, K., Lu, Y., Wang, X., Zhao, Y., Bruns, Christiane J., et al. (2016). PHF20 Readers Link Methylation of Histone H3K4 and p53 with H4K16 Acetylation. *Cell Reports* 17, 1158-1170. <https://doi.org/10.1016/j.celrep.2016.09.056>.
- Klionsky, D.J., and Emr, S.D. (2000). Autophagy as a regulated pathway of cellular degradation. *Science* 290, 1717-1721. 10.1126/science.290.5497.1717.
- Lee, J.E., Wang, C., Xu, S., Cho, Y.W., Wang, L., Feng, X., Baldrige, A., Sartorelli, V., Zhuang, L., Peng, W., and Ge, K. (2013). H3K4 mono- and di-methyltransferase MLL4 is required for enhancer activation during cell differentiation. *Elife* 2, e01503. 10.7554/eLife.01503.
- Levine, B., and Kroemer, G. (2008). Autophagy in the pathogenesis of disease. *Cell* 132, 27-42. 10.1016/j.cell.2007.12.018.
- Li, B., and Dewey, C.N. (2011). RSEM: accurate transcript quantification from RNA-Seq data with or without a reference genome. *BMC Bioinformatics* 12, 323. 10.1186/1471-2105-12-323.
- Li, H., and Durbin, R. (2009). Fast and accurate short read alignment with Burrows-Wheeler transform. *Bioinformatics* 25, 1754-1760. 10.1093/bioinformatics/btp324.
- Li, W., Notani, D., Ma, Q., Tanasa, B., Nunez, E., Chen, A.Y., Merkurjev, D., Zhang, J., Ohgi, K., Song, X., et al. (2013). Functional roles of enhancer RNAs for oestrogen-dependent transcriptional activation. *Nature* 498, 516-520. 10.1038/nature12210.
- Li, X., Wu, L., Corsa, C.A., Kunkel, S., and Dou, Y. (2009). Two mammalian MOF complexes regulate transcription activation by distinct mechanisms. *Mol Cell* 36, 290-301.

10.1016/j.molcel.2009.07.031.

Liberzon, A., Birger, C., Thorvaldsdottir, H., Ghandi, M., Mesirov, J.P., and Tamayo, P. (2015). The Molecular Signatures Database (MSigDB) hallmark gene set collection. *Cell Syst* 1, 417-425. 10.1016/j.cels.2015.12.004.

Liberzon, A., Subramanian, A., Pinchback, R., Thorvaldsdottir, H., Tamayo, P., and Mesirov, J.P. (2011). Molecular signatures database (MSigDB) 3.0. *Bioinformatics* 27, 1739-1740. 10.1093/bioinformatics/btr260.

Liu, R., Gao, J., Yang, Y., Qiu, R., Zheng, Y., Huang, W., Zeng, Y., Hou, Y., Wang, S., Leng, S., et al. (2018). PHD finger protein 1 (PHF1) is a novel reader for histone H4R3 symmetric dimethylation and coordinates with PRMT5-WDR77/CRL4B complex to promote tumorigenesis. *Nucleic Acids Res* 46, 6608-6626. 10.1093/nar/gky461.

Liu, Y., Qin, S., Chen, T.Y., Lei, M., Dhar, S.S., Ho, J.C., Dong, A., Loppnau, P., Li, Y., Lee, M.G., and Min, J. (2019). Structural insights into trans-histone regulation of H3K4 methylation by unique histone H4 binding of MLL3/4. *Nat Commun* 10, 36. 10.1038/s41467-018-07906-3.

Love, M.I., Huber, W., and Anders, S. (2014). Moderated estimation of fold change and dispersion for RNA-seq data with DESeq2. *Genome Biol* 15, 550. 10.1186/s13059-014-0550-8.

Lum, J.J., DeBerardinis, R.J., and Thompson, C.B. (2005). Autophagy in metazoans: cell survival in the land of plenty. *Nat Rev Mol Cell Biol* 6, 439-448. 10.1038/nrm1660.

Mammucari, C., Milan, G., Romanello, V., Masiero, E., Rudolf, R., Del Piccolo, P., Burden, S.J., Di Lisi, R., Sandri, C., Zhao, J., et al. (2007). FoxO3 controls autophagy in skeletal

muscle in vivo. *Cell Metab* 6, 458-471. 10.1016/j.cmet.2007.11.001.

Meers, M.P., Bryson, T.D., Henikoff, J.G., and Henikoff, S. (2019). Improved CUT&RUN chromatin profiling tools. *Elife* 8. 10.7554/eLife.46314.

Miller, T., Krogan, N.J., Dover, J., Erdjument-Bromage, H., Tempst, P., Johnston, M., Greenblatt, J.F., and Shilatifard, A. (2001). COMPASS: a complex of proteins associated with a trithorax-related SET domain protein. *Proc Natl Acad Sci U S A* 98, 12902-12907. 10.1073/pnas.231473398.

Milne, T.A., Briggs, S.D., Brock, H.W., Martin, M.E., Gibbs, D., Allis, C.D., and Hess, J.L. (2002). MLL Targets SET Domain Methyltransferase Activity to Hox Gene Promoters. *Molecular Cell* 10, 1107-1117. [https://doi.org/10.1016/S1097-2765\(02\)00741-4](https://doi.org/10.1016/S1097-2765(02)00741-4).

Mizushima, N. (2007). Autophagy: process and function. *Genes Dev* 21, 2861-2873. 10.1101/gad.1599207.

Mizushima, N., Levine, B., Cuervo, A.M., and Klionsky, D.J. (2008). Autophagy fights disease through cellular self-digestion. *Nature* 451, 1069-1075. 10.1038/nature06639.

Naumova, N., Smith, E.M., Zhan, Y., and Dekker, J. (2012). Analysis of long-range chromatin interactions using Chromosome Conformation Capture. *Methods* 58, 192-203. 10.1016/j.ymeth.2012.07.022.

Oh, S., Boo, K., Kim, J., Baek, S.A., Jeon, Y., You, J., Lee, H., Choi, H.J., Park, D., Lee, J.M., and Baek, S.H. (2020). The chromatin-binding protein PHF6 functions as an E3 ubiquitin ligase of H2BK120 via H2BK12Ac recognition for activation of trophectodermal genes. *Nucleic Acids Res* 48, 9037-9052. 10.1093/nar/gkaa626.

Patel, A., Dharmarajan, V., Vought, V.E., and Cosgrove, M.S. (2009). On the mechanism

of multiple lysine methylation by the human mixed lineage leukemia protein-1 (MLL1) core complex. *J Biol Chem* 284, 24242-24256. 10.1074/jbc.M109.014498.

Patel, A., Vought, V.E., Dharmarajan, V., and Cosgrove, M.S. (2011). A novel non-SET domain multi-subunit methyltransferase required for sequential nucleosomal histone H3 methylation by the mixed lineage leukemia protein-1 (MLL1) core complex. *J Biol Chem* 286, 3359-3369. 10.1074/jbc.M110.174524.

Quinlan, A.R., and Hall, I.M. (2010). BEDTools: a flexible suite of utilities for comparing genomic features. *Bioinformatics* 26, 841-842. 10.1093/bioinformatics/btq033.

Ramirez, F., Ryan, D.P., Gruning, B., Bhardwaj, V., Kilpert, F., Richter, A.S., Heyne, S., Dundar, F., and Manke, T. (2016). deepTools2: a next generation web server for deep-sequencing data analysis. *Nucleic Acids Res* 44, W160-165. 10.1093/nar/gkw257.

Settembre, C., Di Malta, C., Polito, V.A., Garcia Arencibia, M., Vetrini, F., Erdin, S., Erdin, S.U., Huynh, T., Medina, D., Colella, P., et al. (2011). TFEB links autophagy to lysosomal biogenesis. *Science* 332, 1429-1433. 10.1126/science.1204592.

Shia, W.J., Pattenden, S.G., and Workman, J.L. (2006). Histone H4 lysine 16 acetylation breaks the genome's silence. *Genome Biol* 7, 217. 10.1186/gb-2006-7-5-217.

Shilatifard, A. (2012). The COMPASS family of histone H3K4 methylases: mechanisms of regulation in development and disease pathogenesis. *Annu Rev Biochem* 81, 65-95. 10.1146/annurev-biochem-051710-134100.

Shin, H.J., Kim, H., Oh, S., Lee, J.G., Kee, M., Ko, H.J., Kweon, M.N., Won, K.J., and Baek, S.H. (2016). AMPK-SKP2-CARM1 signalling cascade in transcriptional regulation of autophagy. *Nature* 534, 553-557. 10.1038/nature18014.

- Smedley, D., Haider, S., Ballester, B., Holland, R., London, D., Thorisson, G., and Kasprzyk, A. (2009). BioMart--biological queries made easy. *BMC Genomics* *10*, 22. 10.1186/1471-2164-10-22.
- Smith, E., Lin, C., and Shilatifard, A. (2011). The super elongation complex (SEC) and MLL in development and disease. *Genes Dev* *25*, 661-672. 10.1101/gad.2015411.
- Steward, M.M., Lee, J.S., O'Donovan, A., Wyatt, M., Bernstein, B.E., and Shilatifard, A. (2006). Molecular regulation of H3K4 trimethylation by ASH2L, a shared subunit of MLL complexes. *Nat Struct Mol Biol* *13*, 852-854. 10.1038/nsmb1131.
- Subramanian, A., Tamayo, P., Mootha, V.K., Mukherjee, S., Ebert, B.L., Gillette, M.A., Paulovich, A., Pomeroy, S.L., Golub, T.R., Lander, E.S., and Mesirov, J.P. (2005). Gene set enrichment analysis: a knowledge-based approach for interpreting genome-wide expression profiles. *Proc Natl Acad Sci U S A* *102*, 15545-15550. 10.1073/pnas.0506580102.
- Taipale, M., Rea, S., Richter, K., Vilar, A., Lichter, P., Imhof, A., and Akhtar, A. (2005). hMOF histone acetyltransferase is required for histone H4 lysine 16 acetylation in mammalian cells. *Mol Cell Biol* *25*, 6798-6810. 10.1128/MCB.25.15.6798-6810.2005.
- Thakore, P.I., D'Ippolito, A.M., Song, L., Safi, A., Shivakumar, N.K., Kabadi, A.M., Reddy, T.E., Crawford, G.E., and Gersbach, C.A. (2015). Highly specific epigenome editing by CRISPR-Cas9 repressors for silencing of distal regulatory elements. *Nat Methods* *12*, 1143-1149. 10.1038/nmeth.3630.
- Wang, D., Garcia-Bassets, I., Benner, C., Li, W., Su, X., Zhou, Y., Qiu, J., Liu, W., Kaikkonen, M.U., Ohgi, K.A., et al. (2011). Reprogramming transcription by distinct

classes of enhancers functionally defined by eRNA. *Nature* 474, 390-394. 10.1038/nature10006.

Wang, P., Lin, C., Smith, E.R., Guo, H., Sanderson, B.W., Wu, M., Gogol, M., Alexander, T., Seidel, C., Wiedemann, L.M., et al. (2009). Global analysis of H3K4 methylation defines MLL family member targets and points to a role for MLL1-mediated H3K4 methylation in the regulation of transcriptional initiation by RNA polymerase II. *Mol Cell Biol* 29, 6074-6085. 10.1128/MCB.00924-09.

Yang, Z., and Klionsky, D.J. (2010). Eaten alive: a history of macroautophagy. *Nat Cell Biol* 12, 814-822. 10.1038/ncb0910-814.

Yu, Y.S., Shin, H.R., Kim, D., Back, S.A., Choi, S.A., Ahn, H., Shamim, A., Kim, J., Kim, I.S., Kim, K.K., et al. (2020). Pontin arginine methylation by CARM1 is crucial for epigenetic regulation of autophagy. *Nat Commun* 11, 6297. 10.1038/s41467-020-20080-9.

Yun, M., Wu, J., Workman, J.L., and Li, B. (2011). Readers of histone modifications. *Cell Res* 21, 564-578. 10.1038/cr.2011.42.

Zhang, T., Ah Park, K., Li, Y., Sun Byun, H., Jeon, J., Lee, Y., Hee Hong, J., Man Kim, J., Huang, S.-M., Choi, S.-W., et al. (2013). PHF20 regulates NF- κ B signalling by disrupting recruitment of PP2A to p65. *Nature Communications* 4, 2062. 10.1038/ncomms3062.

Zhang, X., Peng, D., Xi, Y., Yuan, C., Sagum, C.A., Klein, B.J., Tanaka, K., Wen, H., Kutateladze, T.G., Li, W., et al. (2016). G9a-mediated methylation of ER α links the PHF20/MOF histone acetyltransferase complex to hormonal gene expression. *Nat Commun* 7, 10810. 10.1038/ncomms10810.

Zhang, Y., Liu, T., Meyer, C.A., Eeckhoutte, J., Johnson, D.S., Bernstein, B.E., Nusbaum,

C., Myers, R.M., Brown, M., Li, W., and Liu, X.S. (2008). Model-based analysis of ChIP-Seq (MACS). *Genome Biol* 9, R137. 10.1186/gb-2008-9-9-r137.

Zhou, J., Liao, W., Yang, J., Ma, K., Li, X., Wang, Y., Wang, D., Wang, L., Zhang, Y., Yin, Y., et al. (2012). FOXO3 induces FOXO1-dependent autophagy by activating the AKT1 signaling pathway. *Autophagy* 8, 1712-1723. 10.4161/auto.21830.

국문 초록 / ABSTRACT IN KOREAN

오토파지는 세포내 항상성을 유지하기 위해 불필요한 단백질이나 손상된 소기관을 제거하는 작용으로 영양 결핍 상황과 같은 세포 스트레스 상황에서 오토파지는 매우 높은 수준으로 증가하여 세포를 보호하는 역할을 수행한다. 오토파지는 세포의 생존이나 외부 환경으로부터의 피해를 보호하는데 중요한 역할을 수행하므로, 오토파지가 제대로 일어나지 않는 경우 당뇨, 암, 신경퇴행질환과 같은 심각한 질병이 유발된다. 오토파지가 진행됨에 따라, 오토파고좀을 형성하는 단백질 구성성분들은 라이소좀에 의해 급격히 분해되기 시작한다. 따라서 스트레스 상황에서 오토파고좀의 생성과 충분한 오토파지 흐름을 유지하기 위해서는 오토파고좀 구성 단백질들의 유전자 발현이 증가되어야 한다.

유전자 발현은 전사인자들 뿐 아니라 크로마틴 리모델링 인자들에 의해 변형되는 크로마틴 구조를 통해서도 조절된다. 히스톤 꼬리에 일어나는 전사 후 변형과정들은 종류에 따라 전사 활성 혹은 억제와 연관된 크로마틴 구조 변화를 촉진시킨다. 활성화된 프로모터 부위는 H3K4me3로 표시되어 있고 활성화된 인핸서 부위는 H3K4me1 혹은 H3K27ac 와 연관되어 있으며 헤테로크로마틴 부위는 H3K9me3로 표시되어 있다. 특정한 히스톤 표지를 유도하거나 제거하는 효소들은 다양한 세포 상태에 적합한 히스톤 변형을 유도하기 위해 매우 엄격하게 조절된다. 예를 들어, 포도당 결핍 상황에서 H3R17me2는 coactivator-associated arginine methyltransferase 1 (CARM1)에 의해 유도되며 이를 통해 TFEB의 목표 유전자들을 활성화시킨다. 반면 포도당 결핍상황에서 일어나는 males absent on the

first (MOF)의 히스톤 아세틸화 활성 감소와 sirtuin 1의 활성화로 인해 히스톤 H4K16ac은 감소한다. 이와 같은 효소의 작용뿐 아니라 후성유전학적 인지 단백질들이 특정한 히스톤 변형을 인식하고 다른 구조체들을 해당 부위로 불러온다는 점에서, 후성유전적 인지 단백질들의 작용 기전을 밝히는 것 역시 오토파지 유전자 조절의 통합적인 이해를 위해 반드시 필요하지만 현재까지는 많은 연구가 진행되어 있지 않은 상황이다.

PHF 계열 단백질 중 하나인 PHF20은 두개의 Tudor 도메인과 하나의 planthomeodomain (PHD)을 가지고 있다. MOF-nonspecific lethal (NSL) 복합체의 핵심 구성 인자중 하나로써, PHF20은 히스톤 혹은 히스톤 외 다른 전사 조절 단백질의 메틸화를 인지하여 목표 프로모터로 NSL 복합체를 위치시키고 해당 부위에 히스톤 H4 아세틸화를 유도하는 것이 알려져 있다. PHF20 결손 마우스의 경우 대부분 태어난 지 얼마 지나지 않아 사망하며 생존한 성체도 야생형에 비해 상대적으로 작은 크기를 나타내는데 흥미롭게도 오토파지가 제대로 일어나지 않는 마우스에서도 유사한 표현형이 나타난다.

이 연구를 통해, PHF20 결손이 포도당 결핍 상황에서 오토파지를 유지하는데 문제를 일으킨다는 것을 밝히고 오토파지 상황에서 PHF20의 후성 유전적 조절 과정을 새롭게 밝혔다.

주요어: PHF20, 오토파지, 포도당 결핍, 히스톤 변형, 히스톤 메틸화, H3K36me2, H3K4me1/2, MLL 복합체, 인헨서, 후성유전학적 유전자 발현 조절, 차세대 지놈 시퀀싱

학번: 2015-20429